IFT-UAM/CSIC-07-60
CERN-PH-TH/2007-225

Flat Tree-level Inflationary Potentials in Light of CMB and LSS Data

G. Ballesteros [a,b,1], **J. A. Casas** [a,2] **J. R. Espinosa** [a,3],
R. Ruiz de Austri [a,c,4] and **R. Trotta** [d,5]

[a] *IFT-UAM/CSIC, UAM, Cantoblanco, 28049 Madrid, Spain*

[b] *CERN, Theory Division, CH-1211 Geneva 23, Switzerland*

[c] *Dept. de Física Teórica, UAM, Cantoblanco, 28049 Madrid, Spain*

[d] *Oxford University, Astrophysics Department, Denys Wilkinson Building, Keble Road, Oxford OX1 3RH, UK*

Abstract

We use cosmic microwave background and large scale structure data to test a broad and physically well-motivated class of inflationary models: those with flat tree-level potentials (typical in supersymmetry). The non-trivial features of the potential arise from radiative corrections which give a simple logarithmic dependence on the inflaton field, making the models very predictive. We also consider a modified scenario with new physics beyond a certain high-energy cut-off showing up as non-renormalizable operators (NRO) in the inflaton field. We find that both kinds of models fit remarkably well CMB and LSS data, with very few free parameters. Besides, a large part of these models naturally predict a reasonable number of e–folds. A robust feature of these scenarios is the smallness of tensor perturbations ($r \lesssim 10^{-3}$). The NRO case can give a sizeable running of the spectral index while achieving a sufficient number of e–folds. We use Bayesian model comparison tools to assess the relative performance of the models. We believe that these scenarios can be considered as a standard physical class of inflationary models, on a similar footing with monomial potentials.

[1]guillermo.ballesteros@uam.es, [2]alberto.casas@uam.es, [3]jose.espinosa@cern.ch,
[4]rruiz@delta.ft.uam.es, [5]rxt@astro.ox.ac.uk

1 Introduction

The WMAP 3–years data [1,2] on the cosmic microwave background radiation (CMB) represent a milestone in the history of observational cosmology due to their great precision. The challenge for theoretical cosmology and particle physics is to understand these data within some theoretical framework and to make predictions to be tested by future observations. In this respect, inflation stands as the most successful and promising theoretical scenario. Proposed in 1981 as a solution to the flatness and horizon problems [3] it was later shown to predict an almost scale invariant spectrum of matter perturbations [4–8], making it a very successful idea. However, we still lack a concrete description of the mechanism producing inflation in the very early universe. The simplest implementation postulates a real scalar field, ϕ, whose homogeneous part drives inflation during its way towards the minimum of its potential, $V(\phi)$. Therefore, to provide a description of the inflationary epoch of the universe we need to elucidate the functional form of the inflaton potential [9]. In this respect it is fair to say that, despite interesting developments, there is still no convincing inflationary scheme based on particle physics.

The main goal of this work is to compare a broad class of models, which are physically well motivated, with CMB and large scale structure (LSS) data. As shown below, these models predict a scalar spectral index with non-constant slope, in contrast with the ansätze used in standard analyses. Interestingly, these models are very predictive: the number of independent parameters is comparable to the free parameters used in more phenomenological approaches.

This paper is organized as follows. In section 2 we review the standard way of comparing inflationary potentials with cosmological data through parametrizations of the primordial scalar and tensor power spectra that involve the spectral indices and their derivatives (up to a given order). In section 3 we introduce the class of models we are interested in, namely, models with flat tree-level potentials which are generically lifted in a controlled way by radiative corrections. This type of models is then extended by taking into account possible effects from non-renormalizable operators that appear after integrating out some heavy new physics. In both cases we discuss the physical motivation and significance of such models. Section 4 is devoted to the derivation of the power spectra for the two classes of models as a function of suitable model parameters. The data analysis procedure is discussed in section 5; we present parameter constraints within each class of models from our analysis in section 6 while section 7 is devoted to the issue of model comparison, assessing which model is in better agreement with the data. Finally, our conclusions are presented in section 8. In addition, the appendix contains some technical details relevant to the analysis of the model with non-renormalizable operators.

2 Comparing inflationary potentials with data

The usual strategy to probe inflationary potentials is the comparison of theoretical predictions for the spectrum of primordial (scalar and tensor) cosmological perturbations [$P_s(k)$ and $P_t(k)$ respectively, where k stands for the space wave-number] with CMB and

LSS data. This is usually done in the slow-roll approximation [10]. Generically, in this situation $|\epsilon, \eta, \xi| \ll 1$, with

$$\epsilon \equiv \frac{1}{2} M_p^2 \left(\frac{V'}{V}\right)^2 \;, \quad \eta \equiv M_p^2 \frac{V''}{V} \;, \quad \xi \equiv M_p^4 \frac{V'V'''}{V^2} \;, \tag{2.1}$$

where primes denote derivatives with respect to the inflaton ϕ and $M_p \equiv m_p/\sqrt{8\pi}$ (being $m_p \simeq 10^{19}$ GeV) is the reduced Planck mass. In this approximation

$$P_s(k) \simeq \frac{1}{24\pi^2\epsilon} \frac{V}{M_p^4} \,, \tag{2.2}$$

$$P_t(k) \simeq \frac{3}{2\pi^2} \frac{V}{M_p^4} \;. \tag{2.3}$$

Thus the tensor to scalar ratio simply reads

$$r \equiv \frac{P_t}{P_s} \simeq 16\epsilon \,. \tag{2.4}$$

The relationship between the inverse distance scale k and the inflaton field ϕ is given in slow-roll by

$$\frac{d\phi}{d\ln k} \simeq -M_p \sqrt{2\epsilon} \;. \tag{2.5}$$

The number of e-folds between the beginning of inflation (t_*) and the end (t_e) is

$$N_e = \int_{t_*}^{t_e} H dt \simeq \frac{1}{M_p^2} \int_{\phi_e}^{\phi_*} \frac{V}{V'} d\phi = \frac{1}{M_p} \int_{\phi_e}^{\phi_*} \frac{1}{\sqrt{2\epsilon}} d\phi \,, \tag{2.6}$$

where we have used the slow-roll approximation to change variables from t to ϕ. The usual requirement to solve the horizon problem is $N_e \simeq 50 - 60$ although the precise number depends on the details of the post-inflationary epoch [11]. Of course, the total number of e-folds may be much larger, but only 50-60 e-folds are needed and actually WMAP only probes directly the first ~ 7 e-folds, which can be extended to ~ 10 by using LSS data and other observations. Thus the subscript '$*$' above denotes the time at 50-60 e-folds before the end of inflation. On the other hand, there might be several episodes of inflation, in order to achieve the required 50-60 e-folds. In that case, WMAP would be only sensitive to the first(s) of these episodes after t_*.

An important quantity when performing fits to the observations is the scalar spectral index, n, which describes the variation of P_s with k,

$$n - 1 = \frac{d\ln P_s}{d\ln k} \simeq 2\eta - 6\epsilon \;. \tag{2.7}$$

The spectral index itself may change with k:

$$\frac{dn}{d\ln k} \simeq -2\xi + 16\epsilon\eta - 24\epsilon^2 \;. \tag{2.8}$$

The right-hand sides of (2.7) and (2.8) correspond to the slow-roll approximation. Similar equations, involving the tensor spectral index $n_t(k)$, can be written for the variation of $P_t(k)$ with k. Summarizing, observational information about P_s (and thus about n and $dn/d\ln k$) gives information about V and its derivatives, V', V'', V''' and so on, providing a link between theory and experiment.

Standard Parametrizations of the Power Spectrum

A common approach to determining the power spectrum from CMB and LSS data is to perform a Taylor expansion of $\ln P_s(k)$ and $\ln P_t(k)$ in $\ln k/k_0$ around zero, where k_0 is a pivotal scale (from now on fixed to $k_0 \equiv 0.002$ Mpc^{-1}),

$$\ln P_s(k) = \ln P_s(k_0) + [n(k_0) - 1] \ln \frac{k}{k_0} + \frac{1}{2} \frac{dn}{d\ln k}\bigg|_{k_0} \left(\ln \frac{k}{k_0}\right)^2 + \cdots , \tag{2.9}$$

$$\ln P_t(k) = \ln P_t(k_0) + n_t(k_0) \ln \frac{k}{k_0} + \cdots . \tag{2.10}$$

Note from equations (2.2) and (2.4) it follows that, at first order in slow-roll [12]:

$$r(k_0) \equiv \frac{P_t(k_0)}{P_s(k_0)} \simeq -8 n_t(k_0) \ . \tag{2.11}$$

Usually, one does not go beyond the order shown in the equations (2.9) and (2.10). In particular, a running of the tensor spectral index has not been considered because presently the tensor contribution to the spectrum is only weakly constrained by the data. Therefore one typically fits four independent parameters, namely: $\{\ln P_s, n, dn/d\ln k, r\}_{k_0}$ and often the running of the spectral index, $dn/d\ln k|_{k_0}$, and the tensor to scalar ratio, $r(k_0)$, are set to zero. The improvement in the fit obtained when introducing the latter parameters is neither large enough to be considered as a strong indication for their presence nor small enough to be considered as irrelevant. In general, the issue of whether an extra parameter is needed or not is a difficult one and has to be addressed with care, see [13, 14] for a discussion. We return to this question in Section 7.

The Taylor expansion above has been used by the WMAP collaboration. Assuming a ΛCDM universe and setting $dn/d\ln k = r = 0$, WMAP 3–yr data alone give [15]

$$n = 0.958 \pm 0.016 \ , \quad (68\% \text{ c.l.}) \tag{2.12}$$

Including a constant $dn/d\ln k$ the result of the analysis is

$$n(k_0) = 1.050^{+0.059}_{-0.058} \ , \quad (68\% \text{ c.l.}) \tag{2.13}$$

$$\frac{dn}{d\ln k} = -0.055^{+0.030}_{-0.031} \quad (68\% \text{ c.l.}) \, . \tag{2.14}$$

The absolute magnitude of P_s depends slightly on the inflationary model, but roughly one finds $P_s(k_0) \simeq 2 \times 10^{-9}$. The WMAP collaboration used these results to probe monomial potentials $V(\phi) \propto \phi^\alpha$ (with $\alpha = 2, 4$) [2]. These models predict a negligible running of

n, so they are well approximated by equations (2.9) and (2.10) with $dn/d\ln k = 0$. The fits seem to exclude $\alpha = 4$ [16] and any other higher monomial power. The quadratic case, $V = \frac{1}{2}m^2\phi^2$, works quite well, although it requires very large values of the inflaton field, $\phi \sim 14\ M_p$. For the purposes of our discussion it must be stressed that the simple functional forms assumed previously for $P_s(k)$ and $P_t(k)$ may not be accurate enough to describe the actual power spectrum of other inflaton potentials which are well motivated physically. In this sense, although (2.9) and (2.10) can be useful as phenomenological approximations, it is important to be open to other parametrizations. In this paper we will show explicit examples of this. At the end of the day, the best fit together with the best physical motivation will determine the preferred functional form.

3 A broad class of models: Flat Tree-Level Potentials

We will consider models that have "*flat tree-level potentials*" [2], i.e.

$$V_{\rm tree}(\phi) = \rho_{\rm tree} = \text{constant}\ . \tag{3.1}$$

Then, the potential derivatives V', V'',... arise from the radiative corrections to V. These potentials appear typically in supersymmetric (SUSY) theories: $V_{\rm tree}^{\rm SUSY}$ ordinarily has plenty of *accidental* flat directions. A familiar example of this is the minimal supersymmetric standard model (MSSM). Such accidental flatness is broken by radiative corrections since there is no symmetry protecting it. Generically, at one-loop

$$V(\phi) = \rho + \beta\ \ln\frac{m(\phi)}{Q}\ , \tag{3.2}$$

where Q is the renormalization scale (which might have absorbed finite pieces) and $m(\phi)$ is the most relevant ϕ-dependent mass in the spectrum. Note that ρ depends implicitly on Q through its renormalization group equation (RGE) and that the Q-invariance of the effective potential implies

$$\beta = \frac{d\rho}{d\ln Q}\ , \tag{3.3}$$

at one-loop. From now on we will assume $\beta > 0$, which is the usual situation, though the opposite case is also possible and the analysis is similar.

Since these "almost flat" directions are so common in SUSY scenarios, they are natural candidates to drive inflation, provided the potential stores large enough energy density. As a matter of fact, particular examples of these approximate flat directions have been used in the literature to implement inflation, e.g. the first D-hybrid inflation model belongs to this class [18]. The important point is that, whatever the model considered, the slope of $V(\phi)$, and thus the dynamics of inflation, are determined by radiative corrections. Since the latter have a very generic functional form (logarithmic), it is possible to make very

[2] For a more complete discussion of the theoretical aspects of these models see [17].

model-independent predictions without relying on a particular model [17]. Next we work out these statements in a more detailed way.

The leading-log approximation (which amounts to summing up the leading-log contributions to all loops) is implemented in this context by simply taking $Q = m(\phi)$. This choice eliminates the potentially large (and thus dangerous) logarithms, improving the convergence of the perturbative expansion. Then

$$V(\phi) \simeq \rho[Q = m(\phi)] \ . \tag{3.4}$$

In general, one expects $m^2(\phi) = M^2 + c^2\phi^2$, where M does not depend on ϕ, and c is some coupling constant (which depends on Q according to its own RGE). Normally one considers a range of $\phi-$values where either the constant M^2 piece (if it exists) or the $\phi-$dependent part dominate. We assume we are in the second case. Hence, we will ignore the possible presence of M and take $Q = m(\phi) = c\,\phi$.

Logarithmic regime (LOG)

In the regime of very small coupling constants one has $d\beta/d\ln Q \ll \beta$ since the former is higher order in the couplings and has a loop suppression factor. Then we can consider β as constant in the range of $Q \propto \phi$ of interest (which is never too wide). Now the scalar potential (3.4) can be easily written in terms of its value at ϕ_0, the value of the inflaton at k_0, integrating equation (3.3):

$$V(\phi) = \rho_0 + \beta \ \ln\frac{\phi}{\phi_0} \ , \tag{3.5}$$

where $\rho_0 \equiv \rho(\phi_0)$. Note that (3.5) can also be obtained from (3.2) by choosing $Q = c\phi_0$.

Since $\ln\phi = \lim_{\alpha\to 0}\alpha^{-1}(\phi^\alpha - 1)$ the logarithmic potential (3.5) can be considered in many respects as a monomial potential with $\alpha = 0$. In particular all the derivatives, which are crucial for the cosmology of the model, follow that pattern. On the other hand, as argued above, this potential is physically as well motivated as the monomial forms.

Logarithmic regime + non-renormalizable operator (LOG+NRO)

If there is a scale of new physics, M, higher than the scales relevant to inflation (i.e. $M^2 \gg \phi^2$), the new physics will generically show up in the effective theory at lower scales as non-renormalizable operators (NROs) of the light fields, suppressed by inverse powers of M. Due to the suppression factor, the impact of the NROs in the physics at low scales is usually very small. However, if the NRO has characteristics not shared by the low-energy physics, its effect may be significant (as happens with higher-dimension operators that mediate proton decay or give a Majorana mass to neutrinos). In our case, the new physics does not need to respect the accidental flat directions of the effective theory. Thus one expects the inflaton potential (3.5) to become

$$V(\phi) = \rho_0 + \beta\ln\frac{\phi}{\phi_0} + \phi^4\frac{\phi^{2N}}{M^{2N}} \ . \tag{3.6}$$

The first two terms correspond to the generic one-loop potential in the small-coupling regime while the last term is a non-renormalizable operator left in the low-energy theory after integrating out some unspecified physics at the high scale M. Notice that this scale absorbs any possible coupling in front of the operator. Of course $V(\phi)$ may contain other NROs of different order. Here we assume that the one shown in equation (3.6) is the lowest order one, and thus the dominant one. The sign and power we have assumed for this NRO guarantee the stability of the potential. Notice also that an even power for this operator is what one expects generically in supersymmetric theories. An explicit example of this is given in [17]. Apart from that, the potential (3.6) is completely general and therefore the analysis is quite model-independent.

4 Primordial spectra in the slow-roll approximation

4.1 Logarithmic regime (LOG)

From $V(\phi)$, as given in equation (3.5), the first three slow-roll parameters (2.1) in the LOG scenario are

$$\epsilon \simeq \frac{1}{2} q^2 \frac{M_p^2}{\phi^2} \,, \qquad \eta \simeq -q \frac{M_p^2}{\phi^2} \simeq -2\frac{\epsilon}{q} \,, \qquad \xi \simeq 2\eta^2 \,, \tag{4.1}$$

where we have introduced the quantity

$$q \equiv \frac{\beta}{\rho_0} \,. \tag{4.2}$$

Note that $q > 0$ since we have assumed $\beta > 0$. Satisfying the slow-roll condition $\epsilon \ll 1$, requires $q \ll 1$ for $\phi < M_p$. This implies in turn $\epsilon \ll |\eta|$. We give a more quantitative evaluation of this hierarchy in Section 5.

The number of e-folds between time t_0 (i.e. the time when $\phi = \phi_0$) and the end of inflation, t_e, can be easily computed using ϵ, as given by equation (4.1), in the usual expression (2.6):

$$N_e(t_0 \to t_e) \simeq -\frac{1}{2}\left[\frac{1}{\eta(\phi_0)} - \frac{1}{\eta(\phi_e)}\right] \simeq -\frac{1}{2\eta(\phi_0)} \simeq \frac{1}{2}\frac{\phi_0^2}{qM_p^2} \equiv N_e^0 \,, \tag{4.3}$$

where we have used the fact that inflation comes to an end when $\eta \sim \mathcal{O}(1)$ (it could end before that time if inflation is interrupted by other mechanisms, like a waterfall field in hybrid models). The N_e^0 parameter defined above, besides giving an excellent approximation to $N_e(t_0 \to t_e)$, will play a relevant role when performing the fits to the data.

Now the $\phi - k$ connection, equation (2.5), can be integrated at first order in q, giving

$$\phi^2 = \phi_0^2 \left(1 - \frac{1}{N_e^0} \ln \frac{k}{k_0}\right) \,, \tag{4.4}$$

where we have used (4.3). Note that increasing ϕ corresponds to decreasing k so that the scales probed by WMAP correspond to the highest values of ϕ during its slow-roll towards the origin. Now we can straightforwardly evaluate $P_s(k)$ from equation (2.2). For the purpose of comparing the model with the data, it is convenient to write P_s in terms of $P_s^0 \equiv P_s(k_0)$ using the general expression

$$\ln P_s = \ln P_s^0 + 3 \ln \frac{V(\phi)}{V(\phi_0)} - 2 \ln \frac{V'(\phi)}{V'(\phi_0)} \ . \tag{4.5}$$

Using equations (3.5) and (4.4) and expanding in q we find, at first order,

$$\ln P_s(k) = \ln P_s^0 + \left(1 + \frac{3}{2} q\right) \ln \left(1 - \frac{1}{N_e^0} \ln \frac{k}{k_0}\right) \ , \tag{4.6}$$

where, from equation (2.2),

$$P_s^0 = \frac{1}{12\pi^2} \frac{\rho_0^3 \phi_0^2}{M_p^6 \beta^2} \ . \tag{4.7}$$

The same result can be obtained by integrating the slow-roll equation (2.7).

Similarly, the spectrum of tensor perturbations, $P_t(k)$, can be obtained from equation (2.3)

$$P_t(k) \simeq \frac{4 q P_s^0}{N_e^0} \left[1 + \frac{q}{2} \ln \left(1 - \frac{1}{N_e^0} \ln \frac{k}{k_0}\right)\right] \ . \tag{4.8}$$

At the same level of approximation, the tensor-to-scalar ratio (2.4) reads

$$r(k) \simeq \frac{4q}{N_e^0} \left(1 - \frac{1}{N_e^0} \ln \frac{k}{k_0}\right)^{-1} \ . \tag{4.9}$$

Let us now count the number of independent parameters. The power spectra, $P_s(k)$ and $P_t(k)$, contain three independent parameters, $\{P_s^0,\, q,\, N_e^0\}$, which are combinations of the initial parameters $\{\phi_0,\, \rho_0,\, \beta\}$. Incidentally note that the scalar potential (3.5) is a function of just two combinations of parameters, but a third one appears in the conversion of ϕ into k through equation (4.4). Actually, the q term in (4.6) is subdominant because $q \ll 1$. Removing it from the expression is a good approximation and eliminates one parameter. So the expression of $P_s(k)$ contains basically two parameters. This is to be compared with the three parameters (two if the running of n is set to zero) of the simple standard parametrization (2.9). As a consequence this LOG scenario is highly predictive. On the other hand, the fits to WMAP data prefer $P_t(k) \ll P_s(k)$, which means that P_t turns out to be scarcely important in the fit, and so the number of relevant parameters continues to be two. Indeed, from equation (4.9) and $q \ll 1$ we do expect by construction $P_t(k) \ll P_s(k)$, something that cannot be postulated from the simple parametrizations (2.9) and (2.10), which contain the additional parameter $P_t(k_0)$ or, equivalently, r (unless r is set to zero by hand).

Equations (4.6) and (4.8) summarize the predictions of models with flat tree-level potentials in the small coupling regime. It is possible to gain some intuition about the

performance of these functional forms as follows. As mentioned above, $\epsilon \ll |\eta|$, which means $n - 1 \simeq 2\eta$. Therefore [see equation (4.1)],

$$\frac{dn}{d\ln k} \simeq -2\xi = -(n-1)^2 \ . \tag{4.10}$$

As a consequence, $dn/d\ln k$ is negative, as suggested by the data, though its value tends to be quite small. In fact the sign of $n-1$ cannot change along the inflationary process in this class of models. Since the dependence of n on the scale is weak, and therefore $n \simeq$ constant, we can expect a fit similar to the one obtained by using the standard parametrization of equation (2.9) with $dn/d\ln k = 0$, leading to $n_0 \sim 0.95$. We will see in Section 5 that this is indeed the case.

Equation (4.10) can be written in an integrated form as

$$n = 1 - \frac{1}{N_e^0 - \ln(k/k_0)} \ , \tag{4.11}$$

where we have used equation (4.3). Equation (4.11) is the prediction for the spectral index in scenarios with flat tree-level potential in the regime of small coupling. It can be compared with the $n =$ constant or $dn/d\ln k =$ constant assumptions made in standard analyses. Note that N_e^0 is the only independent parameter in (4.11) and has a precise physical meaning.

4.2 Logarithmic regime and non–renormalizable operator (LOG + NRO)

In this scenario the derivatives of the potential $V(\phi)$ [equation (3.6)] with respect to ϕ read

$$\begin{aligned} V'(\phi) &= \frac{\beta}{\phi} + 2(N+2)\phi^3\frac{\phi^{2N}}{M^{2N}} \ , \\ V''(\phi) &= -\frac{\beta}{\phi^2} + 2(N+2)(2N+3)\phi^2\frac{\phi^{2N}}{M^{2N}} \ , \\ V'''(\phi) &= 2\frac{\beta}{\phi^3} + 4(N+2)(2N+3)(N+1)\phi\frac{\phi^{2N}}{M^{2N}} \ . \end{aligned} \tag{4.12}$$

The corresponding expressions for ϵ, η are

$$\begin{aligned} \epsilon &= \frac{1}{2}\frac{M_p^2}{\phi^2}\left[\frac{\beta}{\rho_0} + 2(N+2)\frac{\phi^4}{\rho_0}\frac{\phi^{2N}}{M^{2N}}\right]^2 \ , \\ \eta &= \frac{M_p^2}{\phi^2}\left[-\frac{\beta}{\rho_0} + 2(N+2)(2N+3)\frac{\phi^4}{\rho_0}\frac{\phi^{2N}}{M^{2N}}\right] \ . \end{aligned} \tag{4.13}$$

In consequence the NRO can have a significant impact on inflation when the small number $(\phi/M)^{2N}$ is comparable in size to β/ϕ^4. It is also immediate to realize from equations (4.12, 4.13) that, for sufficiently large ϕ, the higher derivatives V'', V''' (and thus η, ξ) can

receive a large contribution from the NRO while the contribution to V' (and thus ϵ) is much less significant, thanks to the additional $(2N+3)$ and $(2N+3)(2N+2)$ factors in V'', V'''. Therefore, one expects modifications of the spectral index, n, and its running $dn/d\ln k$ (which depend on η, ξ), especially at the initial scales (very small k and thus large ϕ), and much smaller changes in ϵ (and hence in N_e).

Let us now calculate the expression of the power spectrum $P_s(k)$ in this scenario. As in the previous subsection, we start with the general expression (4.5) where $V(\phi)$ and $V'(\phi)$ are given now by equations (3.6) and (4.12) respectively, and

$$P_s^0 = \frac{1}{12\pi^2}\frac{[V(\phi_0)]^3}{M_p^2[V'(\phi_0)]^2} \ . \tag{4.14}$$

Next we have to convert ϕ into k by integrating equation (2.5). This is done in the Appendix in an exact way. The corresponding formula, equation (A.1), is rather cumbersome. However, using $|q| \ll 1$, one can write the much simpler but extremely accurate expression

$$\ln\frac{k}{k_0} \simeq -\varphi N_e^0 \ {}_2F_1\left[\frac{1}{N+2}, 1; \frac{N+3}{N+2}; -\left(A\varphi\right)^{N+2}\right]\Bigg|_{\varphi=1}^{\phi^2/\phi_0^2} , \tag{4.15}$$

where ${}_2F_1(a,b;c;z)$ is the Gauss' hypergeometric function [19], φ is just a dummy variable and

$$A^{N+2} \equiv 2(N+2)\frac{\phi_0^4}{\beta}\frac{\phi_0^{2N}}{M^{2N}} \ . \tag{4.16}$$

Note that N_e^0 is still defined as in equation (4.3) and gives a good estimate of the number of e-folds $N_e(t_0 \to t_e)$. It is possible to invert (4.15) numerically to get $\phi = \phi(k)$. Plugging $\phi(k)$ into equation (4.5) we obtain $P_s(k)$. This is the procedure we have followed in doing the fits. Using $\phi(k)$ we can also obtain other quantities of interest as functions of k, e.g. the spectral index $n \simeq 1 + 2\eta - 6\epsilon$ or the tensor to scalar ratio $r \simeq 16\epsilon$.

In order to get some intuition about the shapes of $P_s(k)$ and $n(k)$ it is convenient to derive an analytical approximation to the previous numerical procedure. Actually the numerical part just comes from the ϕ to k conversion, i.e. the integration of equation (2.5). This equation depends on ϵ (on V and V') but not on higher derivatives of V, which are the ones most affected by the presence of the NRO, as discussed after equation (4.12). Therefore it is sensible to use here the value of ϵ when the NRO is switched off, i.e. that of equation (4.1). Then the ϕ to k relation is still given by equation (4.4). Substituting this in the general expression for $P_s(\phi)$, equation (4.5), and expanding at first order in the NRO contributions, one gets[3]

$$\ln\frac{P_s(k)}{P_s^0} \simeq \left(1+\frac{3}{2}q\right)\ln\left(1-\frac{1}{N_e^0}\ln\frac{k}{k_0}\right) + \frac{\gamma N_e^0}{N+2}\left[1-\left(1-\frac{1}{N_e^0}\ln\frac{k}{k_0}\right)^{N+2}\right] , \tag{4.17}$$

[3] This approximate formula gives $P_s(k)$ with a maximum error of $\lesssim 13\%$ in the most extreme cases although typically is much better. Anyway, we remark that in the fit we evaluate $P_s(k)$ numerically using equation (4.15).

where

$$\gamma \equiv \left\{ 2N+3+\left[\frac{1}{2(N+2)}-3\right] q + \frac{3}{2(N+2)} q^2 \right\} \frac{A^{N+2}}{N_e^0} \approx (2N+3)\frac{A^{N+2}}{N_e^0} \,. \qquad (4.18)$$

The approximate equality in the last expression is justified by the smallness of q. Alternatively, one can expand $n-1 \simeq 2\eta - 6\epsilon$ at first order in the NRO and approximate again the ϕ to k conversion by equation (4.4). One obtains

$$n(k) - 1 \simeq -\left(1+\frac{3}{2}q\right)\frac{1}{N_e^0}\left(1-\frac{1}{N_e^0}\ln\frac{k}{k_0}\right)^{-1} + \gamma\left(1-\frac{1}{N_e^0}\ln\frac{k}{k_0}\right)^{N+1} \,. \qquad (4.19)$$

Then the direct integration of (4.19) gives back expression (4.17). Equation (4.19) corresponds to a running $n(k)$ with *non*-constant slope, departing from the assumption of analyses done using the standard parametrization. Unlike in the LOG scenario, in this case the running is not constrained to be very small.

It is also worth mentioning that, due to the positivity of $1-(1/N_e^0)\ln k/k_0$, the sign of the LOG and the NRO contributions to $\{n(k)-1,\ dn/d\ln k,\ d^2n/d\ln^2 k\}$ are $\{-,\ -,\ -\}$ and $\{+,\ -,\ +\}$ respectively [see equation(4.19)]. Since a sizeable running at low k requires a dominant NRO contribution, we can conclude from equation (4.19) that in that case the sign of the second derivative will be positive, although for large enough k it will turn to negative as the LOG part becomes dominant.

In a similar way one can obtain expressions for $P_t(k)$ [or equivalently $r(k)$] starting with the general equations (2.3) or (2.4). In particular, the previous analytical approximation gives in this case

$$r(k) \simeq \frac{4q}{N_e^0}\left(1-\frac{1}{N_e^0}\ln\frac{k}{k_0}\right)^{-1} + \frac{8qA^{N+2}}{N_e^0}\left(1-\frac{q}{2N+4}\right)\left(1-\frac{1}{N_e^0}\ln\frac{k}{k_0}\right)^{N+1} \,. \qquad (4.20)$$

Let us finally count the number of independent parameters. From expressions (4.17) and (4.20) we see that the spectrum of primordial perturbations depends upon five parameters $\{P_s^0,\ N_e^0, q, A, N\}$, which are combinations of the five parameters $\{\rho_0, \beta, \phi_0, M, N\}$ appearing in the scalar potential (3.6). Thus the LOG+NRO has two more parameters than the LOG model. Again, as in the LOG case, the smallness of q implies that $P_s(k)$ is nearly independent of q and, besides, the tensor spectrum is much less important than its scalar counterpart. Hence, q will be irrelevant for a broad range of values in the fit to the data. In practice the primordial spectrum depends essentially on four parameters which become just three if we consider N to be a fixed integer. Again, this is to be compared with the four parameters of the simplest standard parametrizations (2.9) and (2.10). In consequence, the LOG+NRO scenario is still highly predictive.

To illustrate the shapes of the scalar power spectrum in the different scenarios discussed in this section we plot $P_s(k)$ from (4.15) in Figure 1. The parameters for the models are chosen to be the best–fit values given in Section 6 and discussed later in the text.

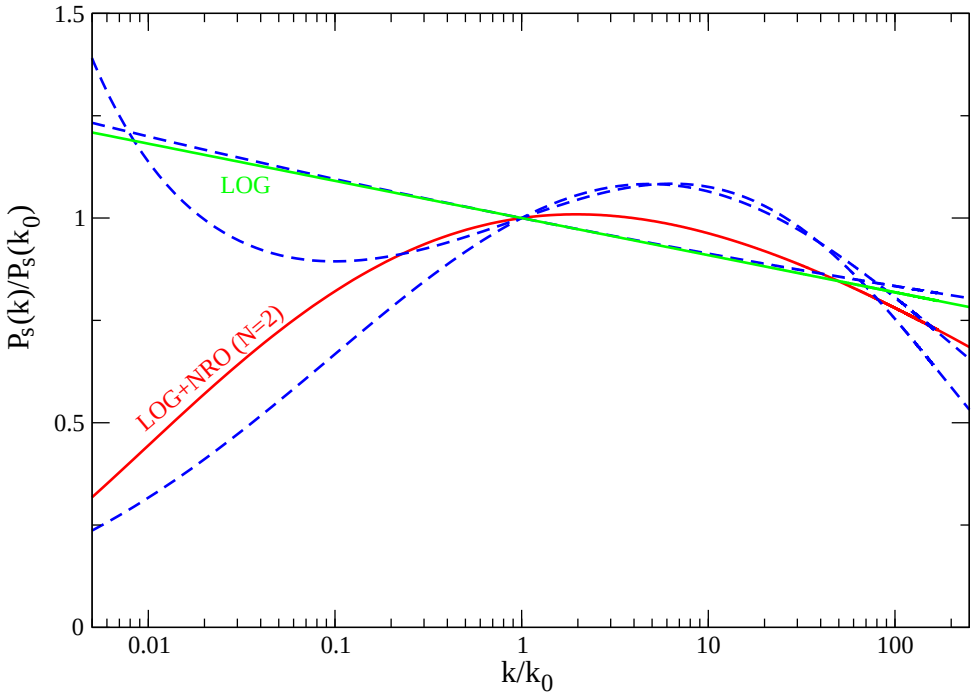

Figure 1: Primordial power spectra in the standard parametrization (dashed lines with Taylor expansion up to second order, i.e. running of running) and as predicted by the LOG and LOG+NRO ($N = 2$) scenarios. Parameters for each case are the best–fit ones (given in Tables 1, 2 and 3).

5 Data analysis procedure

In order to constrain the parameters of the two scenarios introduced above, by comparing their predictions with CMB and LSS data, we use a modified version of the `cosmomc` package [20] with a suitable parametrization of the expressions for $P_s(k)$ and $P_t(k)$. In the next two subsections we describe the detailed procedure for each case separately. We ran six chains for each model, gathering 3×10^5 samples per chain, using the default Metropolis algorithm to sample the parameter space. We discard a burn-in period encompassing the first 10^3 samples in each chain and we employ the usual Raftery and Lewis mixing criterium [21], requiring $R-1<0.1$ for the merged chains.

We consider a flat cosmology, taking flat priors on the cosmological parameters $\Omega_b h^2$, $\Omega_c h^2$ (the baryon and CDM density, respectively), Θ_* (the ratio of the distance to the last scattering surface to the sound horizon) and τ (the optical depth to reionization). We assume dark energy in the form of a cosmological constant ($w=-1$) and 3 species of massless neutrinos. The parametrizations of the primordial power spectrum are discussed in detail below.

We use a combination of CMB and LSS data to constrain the parameters of the models. The main reason for doing so is that it helps to break parameter degeneracies [22]. In particular, we use the latest WMAP [23], ACBAR [24], CBI [25] and BOOMERANG [26] CMB data set releases and the results from the SDSS galaxy survey [27]. We also add the Hubble Space Telescope measurement of the Hubble constant $H_0 = 72\pm8$ km/s/Mpc [28].

5.1 Logarithmic regime (LOG)

As discussed in Section 4.1, the LOG scenario is described by the three independent parameters $\{\rho, \beta, \phi_0\}$, appearing in the scalar potential (3.5). However, for the purpose of comparing the model with data, it is more appropriate to use the following set:

$$\mathbb{P}_{\rm LOG} \equiv \{\, \ln P_s^0, N_e^0, q \,\}\,, \tag{5.1}$$

which are related to the potential parameters by the relations (4.2), (4.3) and (4.7). The inverse transformations are given by

$$\begin{aligned} \phi_0 &= \sqrt{2qN_e^0}\; M_p\;, \\ \rho_0 &= \frac{6\pi^2 q P_s^0}{N_e} M_p^4\;, \\ \beta &= q\frac{6\pi^2 q P_s^0}{N_e} M_p^4\,. \end{aligned} \tag{5.2}$$

The reasons for preferring the set (5.1) over the original potential parameters are the following. First, the fit to WMAP data is very sensitive to the value of $\ln P_s$ at the pivotal scale, which makes it very convenient to use $\ln P_s^0$ as one of the parameters. Second, N_e^0 appears explicitly in the expressions of $P_s(k)$ and $P_t(k)$ [see equations(4.6) and (4.8)]. In addition, N_e^0 has a clear physical meaning, since for small q it simply expresses the

number of e-folds since the time when k_0 crosses out the horizon until the end of inflation. This also makes it possible to impose on it a physically motivated prior for the number of e-folds, as required to solve the homogeneity and flatness problems. Furthermore, we note from equation (4.11) that N_e^0 and the spectral index at k_0 are simply related,

$$n_0 \simeq 1 - \frac{1}{N_e^0} \,. \tag{5.3}$$

Finally, the third parameter, q, does also appear explicitly in the expressions for the spectra. As argued in subsection 4.1, we expect $q \ll 1$, implying that the scalar primordial spectrum depends essentially only on $\{\ln P_s^0, N_e^0\}$, while the tensor spectrum $P_t(k) \simeq 16\epsilon P_s(k)$ is suppressed (and much less important for the fit). Therefore it is convenient to choose q as a parameter for the fit in order to single this effect out. From the above discussion, $\ln P_s^0, N_e^0$ will be well–determined by the observable properties of the power spectrum, and therefore it is appropriate to impose flat priors on them, which corresponds to the assumption that they are location parameters.

The relations between $\mathbb{P}_{\rm LOG}$ and the potential parameters is non–linear and so one expects volume effects coming from the Jacobian of the transformation that will in general make the marginalized constraints on the potential parameters sensitive to the choice of priors. Furthermore, as argued above, only two combinations of parameters of the potential are going to be well determined by the data. The constraints on these "principal directions" in the potential parameter space are however essentially prior–independent, as we discuss in detail in Section 6.2

Let us now focus on the physical constraints on the parameter space spanned by $\mathbb{P}_{\rm LOG}$. The evolution equations of the classical value of the field are based on General Relativity. To prevent effects of quantum gravity from becoming important, we conservatively require the energy density to satisfy

$$\rho < M_p^4 \,. \tag{5.4}$$

Similarly, it is sensible to keep the inflaton field below the Planck scale. Note in particular that, at least in this framework, the renormalization scale Q is to be identified with the value of the inflaton, in order to maintain the radiative corrections under control, and obviously the RGE are only reliable for Q below the Planck scale. Thus we also require, conservatively,

$$\phi_0 < M_p \,. \tag{5.5}$$

Notice that, since the inflaton rolls towards zero, if the above condition is satisfied for ϕ_0 it will automatically be satisfied for smaller values of ϕ, as well. For larger values of ϕ, imposing equation (5.5) easily guarantees that they are well below m_p, since there are very few e-folds before k_0, and they correspond to a short range of ϕ–values.

Moreover, one must ensure that the slow-roll approximation is fulfilled, which means that we require

$$\epsilon < 1 \,, \tag{5.6}$$

$$|\eta| < 1 \,. \tag{5.7}$$

For simplicity we impose these conditions at k_0 and this automatically ensures that the slow-roll is not violated for smaller values of k, which means greater values of ϕ. Therefore the slow-roll will be guaranteed at the scale $k_{obs} \equiv 10^{-4}\text{Mpc}^{-1}$, which is roughly the size of the observable universe. On the other hand, larger values of k are probed and the slow-roll parameters grow as ϕ goes to zero. Taking into account that the largest relevant multipole is about 3000, one gets a maximum k around $k_{max} \equiv 0.1$ Mpc^{-1} [29]. Using equation (4.4), we have checked that slow-roll for such large value of k is indeed satisfied by the samples in our Markov chains. The slow-roll condition on η is equivalent to

$$2N_e^0 > 1\,, \tag{5.8}$$

while the one on ϵ leads to

$$4N_e^0 > q. \tag{5.9}$$

On the other hand, the inequality (5.5) implies

$$2qN_e^0 < 1\,, \tag{5.10}$$

which together with equation (5.8) implies

$$q < 1\,, \tag{5.11}$$

as anticipated in Subsection 4.1.

We found that samples in the Markov chains that fulfill the condition (5.10), automatically satisfy also conditions (5.8), (5.11) and (5.4). This can be understood as follows. As discussed in Subsection 4.1, we expect a value for $n_0 \sim 0.95$, similar to the simplest fit (2.12). Then equation (5.3) implies (5.8). Moreover, the value of n, coupled with the physical prior (5.5), translates into an upper bound on q: since $n-1 \simeq -2\eta \simeq 2q(M_p/\phi_0)^2$, for $\phi_0 \leq M_p$ one gets $q \leq (1-n)/2$, and therefore condition (5.11) holds. Incidentally, this upper bound on q implies that the contribution of the tensor part of the power spectrum must be necessarily small: $r = 16\epsilon \leq 2(1-n)^2$. Finally, (5.4) is granted by the smallness of P_s^0. Notice also that the condition (5.6) on ϵ is, in practice, irrelevant because (5.11) ensures that $\epsilon < |\eta|$, as can also be read off directly from (4.1). In consequence, condition (5.10) remains the only non-trivial constraint.

In summary, we take $\mathbb{P}_{\rm LOG}$ [equation (5.1)] as the set of independent parameters, imposing flat priors on them and enforcing the constraint (5.10). We then compute the scalar and tensor contributions to the primordial spectrum via the expressions (4.6) and (4.8).

As mentioned above, one of the reasons for choosing N_e^0 as an independent parameter is its direct physical interpretation as the number of e-folds. In fact, we have a strong theoretical prejudice about its value, which should be[4]~ 50. We have taken into account this fact by performing two different analyses. The first one imposes a flat prior on N_e^0,

[4]Recall however that its value could be less than 50 if there are subsequent episodes of inflation [see discussion after equation (2.6)]. On the other hand, the parameter N_e^0 [defined in eq. (4.3)] could be larger than 50 if inflation is interrupted e.g. by a waterfall condition in hybrid models [see discussion after equation (4.3)].

therefore assuming no prejudice about its value and leaving the data to constrain it. In the second case we enforce the theoretical requirement by imposing a Gaussian prior on N_e^0 centered on 50 with a standard deviation of 5. The details of these two fits and the results are discussed below, in Subsection 6.2.

5.2 Logarithmic regime and non–renormalizable operator (LOG + NRO)

Concerning the LOG+NRO scenario, for practical reasons it is convenient to work with the set of independent parameters

$$\mathbb{P}_{\rm LOG+NRO} \equiv \{ \ln P_s^0, N_e^0, q\,, A\,, N \}\,, \tag{5.12}$$

where A was defined in equation (4.16), instead of the parameters $\{\rho, \beta, \phi_0, M, N\}$ of the scalar potential (3.5). The relationships between $\mathbb{P}_{\rm LOG+NRO}$ and the potential parameters are given in appendix A.

The convenience and significance of the first three parameters in $\mathbb{P}_{\rm LOG+NRO}$ are the same as in the LOG scenario. However, the interpretation of N_e^0 as the number of e-folds between k_0 and the end of inflation is now less accurate since there are NRO corrections, although it is still a good approximation. This is also true for the connection between N_e^0 and the spectral index n_0: the relation (5.3) becomes now

$$n_0 \simeq 1 - \left(1 + \frac{3}{2}q\right)\frac{1}{N_e^0} + \gamma \simeq 1 - \frac{1}{N_e^0} + (2N+3)\frac{A^{N+2}}{N_e^0}\,. \tag{5.13}$$

This expression tells us that for not too large N_e^0 we should expect A to be bounded from above by some number close to unity because otherwise n_0 can become substantially different from 1 (especially for high values of N), thus violating the slow-roll conditions. This is also illustrated in Figure 2 which shows contour plots for the scalar spectral index and its running at k_0 at lowest order in slow-roll as functions of A and N_e^0 for $N = 2$ and $N = 10$. It is worth remarking here that since we are dealing with scale dependent quantities the appearance of these graphs would change if we made them at a different k. Figure 2 allows to realize that, in the context of the LOG+NRO scenario, it is possible to have simultaneously a sizeable running and a reasonable number of e-folds.

Concerning the physical limits in parameter space, we must take into account the presence of the scale of new physics M. The role played by the Planck mass on the LOG scenario corresponds now to M. To keep the validity of the effective potential (3.6) the inflaton must evolve well below that scale, which should be itself smaller than the Planck scale. Thus, we impose the following conservative limits:

$$2\phi_{obs} < M \leq M_p\ , \tag{5.14}$$

$$\rho < M^4\ . \tag{5.15}$$

Notice that we set the first constraint at $\phi_{obs} \equiv \phi(k_{obs})$ in order to ensure it for any value of ϕ in the observable range.

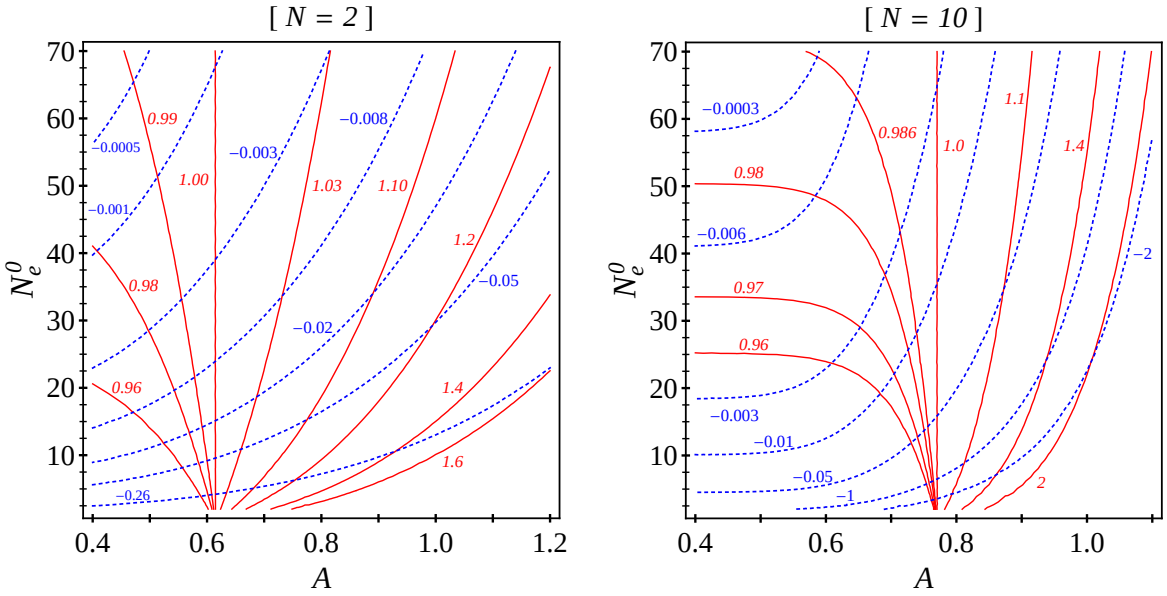

Figure 2: Values of the scalar spectral index (red lines) and its running (blue dashed lines) at k_0 computed at lowest order in slow roll for the LOG+NRO class of models with N as indicated.

As in the LOG scenario, $|\eta| \gg \epsilon$, so η is the relevant parameter for the breakdown of the slow-roll. However, unlike in the LOG case, due to the NRO the absolute value of η grows with sufficiently large ϕ. Therefore we must ensure the fulfilment of slow-roll not only at k_{max} but also at k_{obs}. This guarantees that any point in between will satisfy the slow-roll conditions as well. So, we reject in the Monte Carlo process those points such that

$$|\eta(k_{obs})| > \eta_{\rm lim} \ , \tag{5.16}$$

or

$$\eta(k_{max}) > \eta_{\rm lim} \, , \tag{5.17}$$

being $\eta_{\rm lim}$ a limiting value (smaller than 1) that we set at the beginning of the run. At the end we check that $\eta_{\rm lim}$ was indeed well chosen to ensure the validity of the slow-roll approximation. In practice we work with $\eta_{\rm lim} = 0.2$ which is a rather conservative value. We have checked that the change in the results is negligible if instead we use $\eta_{\rm lim} = 0.5$.

On the other hand, we expect theoretically that the parameter N should be in the range from 1 to $\mathcal{O}(10)$. It is very common that flat directions in supersymmetric models are only lifted by NROs at very high order (as it is the case of the MSSM [30,31]). This is also very common in D=4 string compactifications due to stringy selection rules [32, 33]. For further details see [17]. In Section 6 we discuss in detail two representative cases, which reasonably encompass the range of values for N ($N = 2$ and $N = 10$), and we comment on the qualitative behaviour for values of N in–between.

As for the LOG scenario, we can consider N_e^0 as a free parameter with a flat prior on it or we can alternatively constrain it to be around 50. We have performed the two types of fit.

Finally, we can anticipate theoretically the appearance of some strong bounds on the parameters of the model when performing the fits. First note that the observed power spectrum normalization $P_s^0 \sim 2 \times 10^{-9}$ implies through equation (2.2) the smallness of ρ_0/M_p^4. More precisely

$$\frac{\rho_0}{M_p^4} \simeq 5 \times 10^{-7} \epsilon_0 \ , \tag{5.18}$$

where the subscript "0" indicates evaluation at the pivotal scale. On the other hand, from equations (4.13) we note that the smallness of $|\eta|$ (to preserve the slow-roll) implies that the two contributions within the square brackets (i.e. the LOG and the NRO contributions) must be small separately. Otherwise one should require an unjustified fine-tuned cancellation between them. Actually, even with fine-tuning, one could arrange the parameters to produce the cancellation only at a particular ϕ (and thus k): since the $\phi-$dependence of the two terms is very different, at another (not too distant) value of ϕ the cancellation would not work, spoiling the slow-roll. Consequently, the smallness of $|\eta|$ implies

$$\frac{\beta}{\rho_0} \lesssim \eta_0 \left(\frac{\phi_0}{M_p}\right)^2 \ , \tag{5.19}$$

$$\left(\frac{\phi}{M_p}\right)^{2N+2} \lesssim \frac{|\eta_0|}{2(N+2)(2N+3)} \frac{\rho_0}{M_p^4} \simeq \frac{5 \times 10^{-7} \epsilon_0 |\eta_0|}{2(N+2)(2N+3)} \ , \tag{5.20}$$

In the second equation we have used $M \leq M_p$ and equation (5.18). On the other hand, comparing the two equations (4.13), and recalling that there cannot be fine–tuned cancellations in η, it is clear that

$$\epsilon_0 \lesssim \frac{1}{2} \left(\frac{\phi_0}{M_p}\right)^2 \eta_0^2 \ . \tag{5.21}$$

Using this relation in (5.20) we get

$$\left(\frac{\phi}{M_p}\right)^{2N} \lesssim \frac{5 \times 10^{-7} |\eta_0|^3}{4(N+2)(2N+3)} \ , \tag{5.22}$$

which, substituted into (5.19), gives

$$q = \frac{\beta}{\rho_0} \lesssim |\eta_0|^{1+\frac{3}{N}} \left[\frac{5 \times 10^{-7}}{4(N+2)(2N+3)}\right]^{\frac{1}{N}} \ . \tag{5.23}$$

This shows that q is typically small: for $N = 2$ ($N = 10$) one obtains $q \lesssim 1.7 \times 10^{-6}$ ($q \lesssim 1.4 \times 10^{-2}$), a conservative estimate obtained by replacing $\eta_0 \to \eta_{\rm lim} = 0.2$. In practice η is substantially smaller since the bound $\eta \leq \eta_{\rm lim}$ is to be fulfilled at all k, not just at the pivotal scale. Similar bounds on q can be obtained using our priors together with the constraint $M \leq M_p$. We have checked numerically that the values obtained agree with the ones derived above.

6 Results

6.1 Standard parametrization

The results obtained using the standard parametrization for the primordial spectra [equations (2.9) and (2.10)] are summarized for easy reference in Table 1 both with and without a running spectral index [i.e. including or not the last term of equation (2.9)]. For later reference, we have also considered the next term in the Taylor expansion (2.9), which has been denoted as "running of the running", in the last two columns of Table 1. The table shows the best–fit parameter values, the posterior values and 68% 1-dimensional posterior intervals for the parameters. We also give the best–fit values for (minus twice) the log–likelihood, normalized with respect to the model with only a constant tilt included[5]. Let us recall that the quantities describing the primordial spectrum are defined at $k_0 = 0.002\,\mathrm{Mpc}^{-1}$. These results will be useful later on to interpret the outcomes for the LOG and LOG+NRO models and for the comparison with them.

It is interesting to note that when using the standard parametrization up to second order a large and negative running of the running is preferred [34], which increases the power on large scales (see bottom panel of Figure 4), even though the fit is only marginally better than the case with constant running, see Table 1. This is somewhat surprising: since in the slow-roll approximation $n = 1 + 2\eta - 6\epsilon$, if n departs from scale–invariance too quickly then η, ϵ or both grow up to $\mathcal{O}(1)$ values, marking the end of slow-roll and the inflationary process at quite small k. However, in order to solve the horizon problem we need $\sim 50 - 60$ e-folds of inflation, which corresponds to the same interval in $\ln k$. This requires the (large and negative) $dn/d\ln k$ to get suppressed at some point, suggesting a positive second derivative (unlike the result of the fit). This contradiction could only be avoided if the $n(k)$ function changes abruptly at some point (or, maybe, if there are subsequent episodes of inflation). In any case, it seems clear that the current preference for a negative second derivative is strongly driven by the (possibly anomalous) low power of the large–scale multipoles. This could easily change if observations by Planck do not confirm the lack of large scale power observed by COBE and WMAP. However, we notice that from a model selection perspective even present-day data do not require a non–zero running of the running, as discussed in Section 7. The previous discussion will be useful later on to interpret the outcomes for the LOG and LOG+NRO models and for the comparison with them.

6.2 Logarithmic regime (LOG)

We denote the choice of flat prior on N_e^0 by LOG$\mathcal{F}$, where the top–hat distribution is taken in the interval $2 \leq N_e^0 \leq 1000$. In the second case, denoted by LOG$\mathcal{G}$, we impose a Gaussian prior on N_e^0, with mean 50 and a standard deviation of 5 e-folds. Let us remind

[5]The absolute value of the log–likelihood is of little interest here and in the following. For completeness, we have computed the likelihood values using the WMAP3 likelihood code version v2p2 with the default settings regarding the offset for the log–likelihood. The best–fit value for the constant tilt model is $-2\ln\mathcal{L} = 3614.0$.

Table 1: 1-dimensional marginalized 68% region and best fit values results for the standard parametrizations (2.9), (2.10) with n = constant, $dn/\ln k$ = constant and $d^2n/\ln^2 k$ = constant, from left to right.

Model	no running		with running		running of running	
$-2\Delta \ln \mathcal{L}$	0.0		-3.4		-4.4	
	1D 68%	Best fit	1D 68%	Best fit	1D 68%	Best fit
Cosmological parameters						
$\Omega_b h^2 \times 10^2$	2.23 ± 0.07	2.25	$2.20^{+0.09}_{-0.08}$	2.18	2.22 ± 0.08	2.18
$\Omega_c h^2$	0.106 ± 0.004	0.107	0.107 ± 0.004	0.109	0.107 ± 0.004	0.107
Θ_*	1.043 ± 0.003	1.042	1.043 ± 0.003	1.043	1.044 ± 0.004	1.043
τ	0.084 ± 0.029	0.087	0.114 ± 0.035	0.113	0.106 ± 0.033	0.109
H_0[Km s^{-1}Mpc^{-1}]	74.3 ± 2.1	73.1	73.1 ± 2.3	72.0	73.6 ± 2.4	72.8
Power spectra parameters						
$\ln(P_s^0 \times 10^{10})$	3.11 ± 0.07	3.15	3.00 ± 0.10	3.09	$2.99^{+0.10}_{-0.11}$	3.06
n_0	0.973 ± 0.019	0.961	$1.141^{+0.083}_{-0.082}$	1.085	$1.111^{+0.096}_{-0.091}$	1.069
$\mathrm{d}n/\mathrm{dln}k\big\|_{k_0}$	—	—	-0.07 ± 0.03	-0.06	-0.03 ± 0.07	-0.01
$\mathrm{d}^2n/\mathrm{dln}^2k\big\|_{k_0}$	—	—	—	—	-0.021 ± 0.032	-0.032
r_0	< 0.22	0.003	< 0.59	0.15	< 0.63	0.22

here that N_e^0 approximates the number of e-folds since the time when the scales associated with k_0 first crossed the horizon till the end of inflation. Thus the total number of e-folds since the time when the largest observable scale, k_{obs}, crossed the horizon is $\simeq N_e^0 + 3$. This prior choice incorporates the theoretical prejudice that the total number of e-folds should be in the 50–60 range.

The results of the Monte Carlo Markov chain (MCMC) analysis for the LOG$\mathcal{F}$ and LOG$\mathcal{G}$ cases are given in Figure 3 and are summarized in Table 2. We give 1–dimensional regions encompassing 68% of probability for well–determined parameters; robust upper bounds for parameters whose detailed constraints are parametrization–dependent; and best–fit values. The Table also gives posterior ranges and best–fit values for the corresponding expressions for the tilt, running and tensor–to–scalar ratio at the pivotal scale, n_0, $dn/d\ln k|_0$ and r_0, respectively. These have been obtained by using lowest order expressions in terms of the slow-roll parameters, equations (2.4), (2.7) and (2.8).

As anticipated, constraints on N_e^0 and $\ln P_s^0$ are quite tight, and we have checked that they are almost independent of the choice of prior by performing a run with priors flat in $\{\ln N_e^0, \ln q, \ln P_s^0\}$ instead. It is interesting to notice that in the LOG$\mathcal{F}$ case the 1D 68% (95%) posterior region (2–tails) is approximately $21 < N_e^0 < 46$ ($16 < N_e^0 < 81$), even though the mean is somewhat lower, at around 33 e–folds, and a best–fit around 26 e–folds. This result is close to the theoretical prejudice $N_e^0 \sim 50$, required to solve the horizon problem. Thus assuming a flat tree–level potential for the inflaton, the observed shape of the power spectrum appears to automatically point to model parameters giving a very sensible number of e-folds, in particular given the heavy tail of the probability distribution function (pdf) for large N_e^0. This is not trivial at all: in principle any value for N_e^0 could have emerged from the analysis.

The values of the spectral index and its running at the pivotal scale are easily derived from the parameters of the fit and are also given in Table 2. Note that $dn/d\ln k|_0$ is very small (of order $\sim 10^{-3}$), as expected from the relation (4.10). So the LOG scenario is indeed close to the $n =$ constant limit. The value of n at the pivotal scale, n_0, is directly related to the value of N_e^0 by equation (5.3), leading to the values of n_0 quoted in the Table. The LOG$\mathcal{F}$ best fit value, $n_0 = 0.961$ (corresponding to $N_e^0 = 25.6$), coincides with the value obtained assuming $n =$ constant and negligible running (Table 1). It is interesting to note that although the LOG$\mathcal{F}$ and $n =$ constant fits are very similar, they are not identical, and indeed LOG$\mathcal{F}$ gives a slightly better fit, as can be checked by comparing the best–fit likelihood values (also compare Figure 4). Furthermore, if future CMB and LSS data favour a value of n_0 closer to ~ 0.98, the value of N_e^0 will come out even closer to the theoretically preferred value, $N_e^0 \sim 50$. The upper bound on q is a consequence of the measured tilt and of the physical boundaries imposed on the potential parameters [Recall from the discussion after equation (5.11) that we expect $q \leq (1-n)/2$.] For the reasons explained below, the pdf for q depends on the prior chosen, and therefore we do not show it in Figure 3. However the upper bound is robust with respect to a change of priors, and therefore we chose to report only this value. The tensor contribution remains negligible, below the level $\sim 10^{-3}$, since from (4.9) the value of the tensor-to-scalar ratio

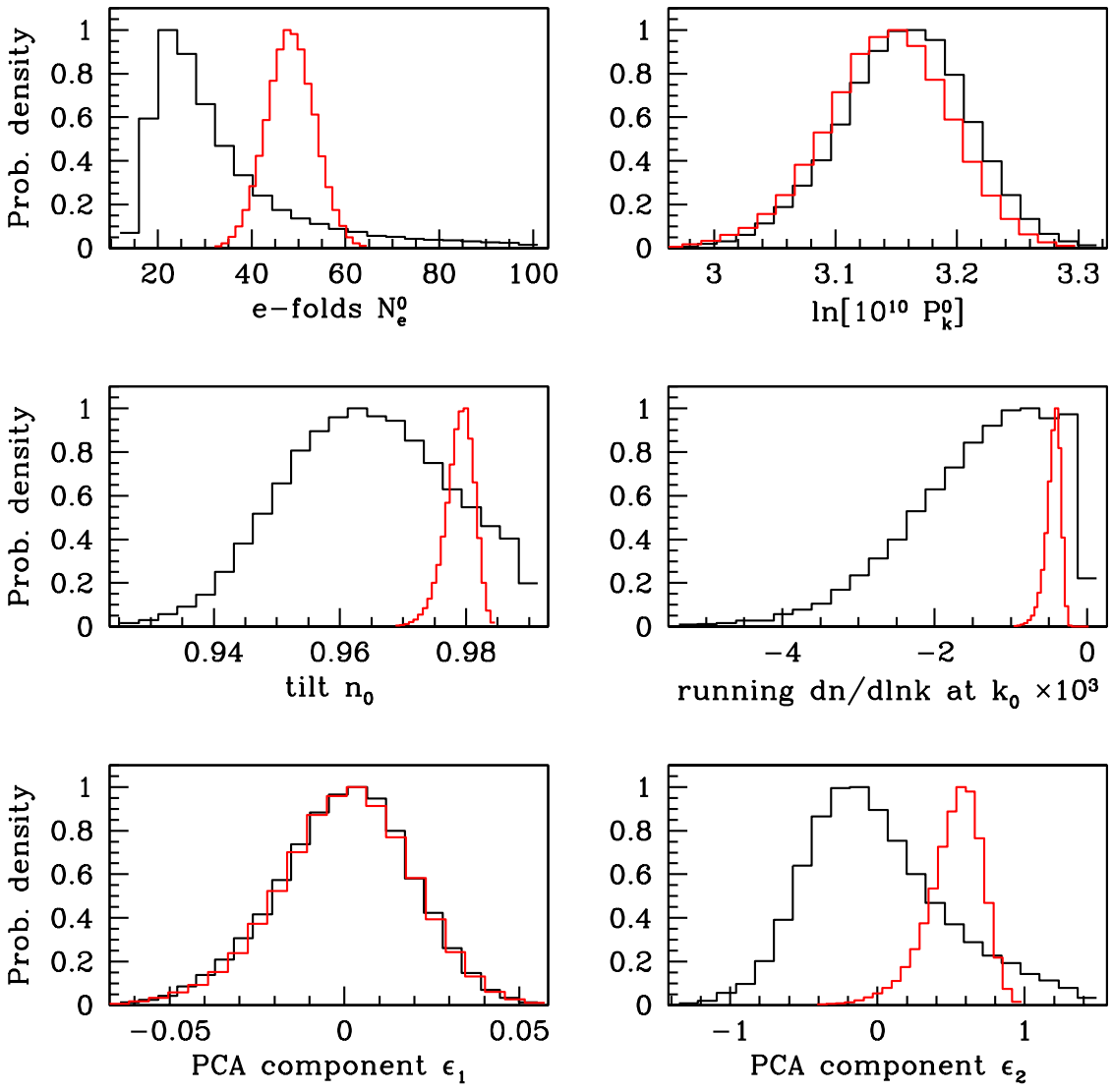

Figure 3: 1D marginalized probability distributions for the well–constrained parameters in the LOG scenario (compare Table 2). Black curves are for the case with a flat prior on N_e^0, while red is for the case where a Gaussian prior around $N_e^0 = 50$ has been enforced.

Table 2: Marginalized 68% regions and best—fit values for the class of models LOG (small–coupling regime) for quantities that are well–determined and essentially prior/parametrization independent. For q and the tensor–to–scalar ratio at the pivotal scale, r_0, we give absolute upper limits that are a consequence of the spectral tilt and of physical priors on the potential parameter space, Eq. (5.5). These bounds have no confidence level attached as the precise numerical value would depend on the prior/parametrization choice, a consequence of the PCA component ε_3 being an unconstrained, degenerate direction in parameter space (see text for details).

Model $-2\Delta \ln \mathcal{L}$	$\boxed{\text{LOG}\mathcal{G}}$ 2.1		$\boxed{\text{LOG}\mathcal{F}}$ -0.4	
	1D 68%	Best fit	1D 68%	Best fit
Cosmological parameters				
$\Omega_b\, h^2 \times 10^2$	2.30 ± 0.04	2.30	2.24 ± 0.07	2.23
$\Omega_c\, h^2$	0.107 ± 0.004	0.1058	0.107 ± 0.004	1.071
Θ_*	1.044 ± 0.003	1.044	1.042 ± 0.003	1.041
τ	0.103 ± 0.026	0.107	$0.089^{+0.028}_{-0.030}$	0.089
H_0 [Km s^{-1}Mpc^{-1}]	74.5 ± 1.5	74.9	73.2 ± 1.9	72.9
Power spectra parameters				
$\ln(P_s^0 \times 10^{10})$	3.14 ± 0.05	3.14	$3.16^{+0.05}_{-0.06}$	3.17
N_e^0	48.3 ± 5.1	48.5	$33.4^{+12.3}_{-12.5}$	25.6
q	< 0.04 for any parametrization			
Derived power spectra parameters				
n_0	0.979 ± 0.002	0.979	$0.964^{+0.016}_{-0.013}$	0.961
$\mathrm{d}n/\mathrm{dln}k\big\vert_{k_0} \times 10^3$	-0.45 ± 0.09	-0.43	-1.42 ± 0.94	-1.54
r_0	$< 4 \times 10^{-3}$ for any parametrization			
Potential parameters and PCA components				
ρ/M_p^4	$< 4 \times 10^{-10}$ for any parametrization			
β/M_p^4	$< 1 \times 10^{-12}$ for any parametrization			
ϕ_0/M_p	< 1 (from prior, Eq. (5.5))			
ε_1	0.00 ± 0.02	0.01	0.00 ± 0.02	0.00
ε_2	0.52 ± 0.18	0.67	0.00 ± 0.48	-0.20
ε_3	essentially unconstrained			

at the pivotal scale is

$$r_0 \simeq 4\frac{q}{N_e^0} \ . \tag{6.1}$$

Consequently the upper bound on q corresponds to an order of magnitude smaller bound on r_0.

The fact that we can extract two measured quantities in this scenario (the tilt and normalization) from three model parameters [either (5.1) or (5.2)] means that we expect a strongly degenerate direction in the primordial power spectrum parameter space. In fact, the constraints coming from the data define a region shaped as a long solid cylinder in the 3D subspace spanned by (5.2). Since this cylinder is not aligned with the potential parameters direction, if one tries to convert limits on (5.1) into limits on the potential parameters (5.2) one unavoidably picks up the degenerate direction, i.e. along the axis of the cylinder. This means that while in the set (5.1) the constraints on $N_e^0, \ln P_s^0$ are robust with respect to a change in the parametrization of the problem (since all the parametrization–dependency is dumped into q), it is impossible to translate these into parametrization–independent results for the potential parameters (5.2).

However, one can still define well–constrained (and parametrization–independent) directions in the subspace spanned by (5.2) by performing a Principal Component Analysis (PCA), i.e. by rotating into a new coordinate system aligned with the degenerate direction. We therefore consider the covariance matrix C in the subspace spanned by the reduced variables $\zeta = (\ln\hat{\rho}_0, \ln\hat{q}, \ln\hat{\phi}_0)$, where hats indicate that the variables have been shifted by their posterior mean and normalized to their posterior standard deviation. Then the PCA vector ε is given by

$$\varepsilon = U\zeta \ , \tag{6.2}$$

where U is the 3D rotation matrix that diagonalizes C:

$$\zeta^t C \zeta = \varepsilon^t \Lambda \varepsilon \ , \tag{6.3}$$

and $\Lambda = \mathrm{diag}(\lambda_1, \lambda_2, \lambda_3)$ is the matrix of eigenvalues, whose square roots give the error along the directions defined by ε. The matrix U is numerically given by

$$U = \begin{pmatrix} 0.46 & -0.68 & 0.57 \\ 0.80 & 0.05 & -0.60 \\ 0.38 & 0.73 & 0.56 \end{pmatrix} \ , \tag{6.4}$$

and $\sqrt{\lambda_1} = 0.02$, $\sqrt{\lambda_2} = 0.48$ while $\sqrt{\lambda_3} \gg 1$, showing that ε_3 is indeed the degenerate direction. We have checked that the constraints on $(\varepsilon_1, \varepsilon_2)$ are largely independent on the chosen parametrization.

The 1-dimensional marginalized probability distributions for the well–constrained parameters in the problem are shown in Figure 3. We do not show the probability distributions for the non–primordial cosmological parameters as they are mostly very similar to the standard scenario, nor do we plot the pdf's for the parameters for which we have only upper limits (q, r_0, ε_3) since their distribution depends on the parametrization employed.

Turning now to the LOG$\mathcal{G}$ case, which imposes a theoretically motivated prior on the number of e–folds, we notice that the prior enforces $N_e^0 \sim 50$. This means that the model

essentially loses one further parameter, and therefore the best–fit log–likelihood is slightly worse (see Table 2). In fact, the LOG$\mathcal{G}$ fit has basically just one free parameter for the power spectrum (namely the normalization $\ln P_s^0$), since q is almost irrelevant. Still, it gives an excellent best fit to observational data! Also, enforcing 50 e–folds results in a very strong prediction for the tilt to be $n_0 \sim 0.98$ (compare Figure 3 and the tightness of the posterior probability for n_0, red curve), while both the tensor contribution and the running are predicted to be very small.

In Figure 4 we plot the CMB temperature power spectrum for the best fit models discussed here along with the compilation of the data used.

6.3 Logarithmic regime and non–renormalizable operator (LOG + NRO)

In this scenario the five parameters we use to describe the primordial spectrum are

$$\mathbb{P}_{\rm LOG+NRO} \equiv \{\ln P_s^0, N_e^0, q\,, A\,, N\}. \tag{6.5}$$

As discussed in Section 5.2, the meaning of the first three ones is similar to those of the LOG case, and we impose flat priors on $\ln P_s^0$ and q. In analogy, we consider two types of fits: LOG+NRO$\mathcal{F}$ (with a flat prior on N_e^0) and LOG+NRO$\mathcal{G}$ (with a Gaussian prior centered at $N_e^0 = 50$ with standard deviation of 5). Since A is expected to be of order unity or less according to the discussion above, it is appropriate to use a flat prior on A between 0 and 1.

Let us recall that N determines the order of the NRO, equation (3.6). As discussed in Section 5.2, we expect it to be within 1 to $\mathcal{O}(10)$. One could imagine treating N as a free parameter and trying to derive a posterior bound on it from the data. However it is technically difficult to ensure that the MCMC is correctly performed across disjoint regions of the parameter space (since N is an integer, using it as a free parameter effectively gives N separated patches across which it is very difficult to sample). Furthermore, NRO's with different values of N are best considered as different models, since the underlying physics is likely to be different. Therefore distinguishing between values of N can be regarded as a model selection task, rather than a parameter constraint exercise. For this reason it is more instructive to consider two separate cases which are representative of the general behaviour at low ($N = 2$) and large ($N = 10$) values of N. Parameter constraints from CMB and LSS data, which are discussed next, are summarized in Table 3 for the $N = 2$ case and in Table 4 for the $N = 10$ case.

Starting from the $N = 2$ case, we find a strong upper bound on q, which reflects the theoretical considerations exposed above and is a consequence of the physically motivated prior (5.14). As a consequence, the tensor contribution is always negligible. The number of e–folds for the LOG+NRO$\mathcal{F}$ case ($N = 2$) is $N_e^0 = 14.5 \pm 3.5$ at 68%, becoming $10.1 \leq N_e^0 \leq 25.8$ at 95%, which is too small to solve the horizon problem. Meanwhile, the parameter A is rather tightly constrained, $A = 0.60^{+0.08}_{-0.09}$. These results can be intuitively understood in the following way. As discussed in Subsection 4.2, the presence of the NRO increases $dn/d\ln k$. This effect is maximal at low k. The lower N is, the more gradual

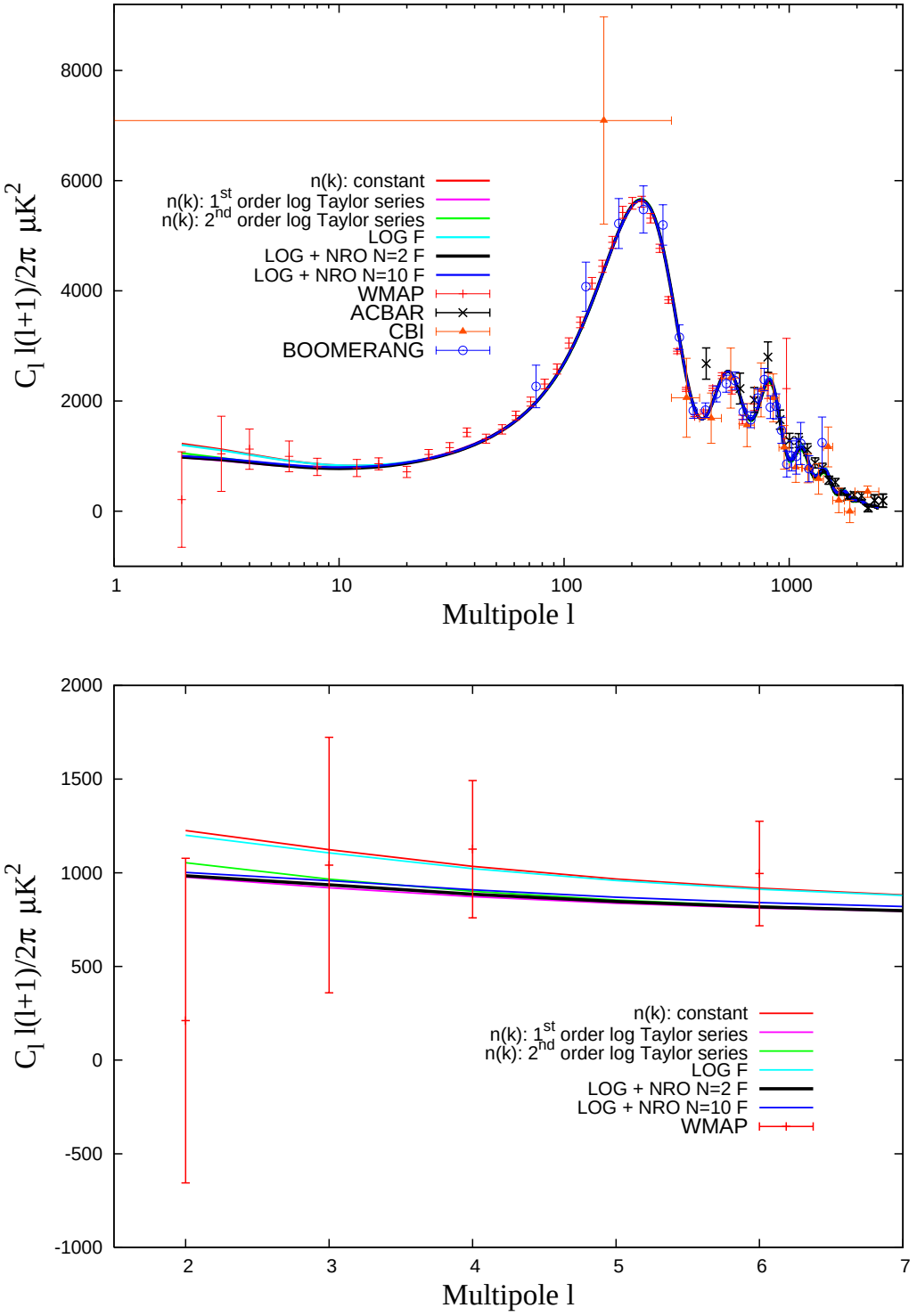

Figure 4: CMB temperature power spectrum for the best–fit model parameters for the standard parametrization, the LOG and the LOG+NRO scenarios. The bottom panel shows the details of the large–scale region.

Table 3: As in Table 1, but for the the class of models referred in the text as LOG+NRO, for $N = 2$. Upper or lower bounds at the specified confidence level are understood to be 1–tail limits.

Model	LOG+NRO$\mathcal{G}$		LOG+NRO$\mathcal{F}$	
$-2\Delta\ln\mathcal{L}$	2.4		-2.7	
	1D 68%	Best fit	1D 68%	Best fit
Cosmological parameters				
$\Omega_b\,h^2\times10^2$	2.32 ± 0.05	2.31	2.18 ± 0.07	2.16
$\Omega_c\,h^2$	0.107 ± 0.004	0.107	0.108 ± 0.004	0.109
Θ_*	$1.044^{+0.003}_{-0.002}$	1.044	1.041 ± 0.003	1.042
τ	0.112 ± 0.026	0.010	0.095 ± 0.030	0.102
H_0 [Km s^{-1}Mpc^{-1}]	$74.7^{+1.6}_{-1.5}$	75.0	$73.3^{+1.9}_{-2.0}$	71.6
Power spectra parameters				
$\ln(P_s^0\times10^{10})$	3.14 ± 0.05	3.13	3.15 ± 0.05	3.15
N_e^0	47.0 ± 5.1	49.6	14.5 ± 3.5	11.7
A	0.46 ± 0.11	0.27	$0.60^{+0.08}_{-0.09}$	0.66
q	$<5\times10^{-6}$ for any parametrization			
Derived power spectra parameters				
n_0	0.987 ± 0.007	0.981	$1.001^{+0.016}_{-0.048}$	1.027
$\mathrm{d}n/\mathrm{dln}k\big\vert_{k_0}\times10^2$	$-0.11^{+0.11}_{-0.05}$	-0.45	$>-6.1\,(95\%)$	-4.28
$\mathrm{d}^2n/\mathrm{dln}^2k\big\vert_{k_0}\times10^3$	0.02 ± 0.02	-0.05	$<14.2\,(95\%)$	7.93
r_0	$<3\times10^{-8}$ for any parametrization			
Potential parameters and PCA components				
ρ/M_p^4	$<1\times10^{-10}$ for any parametrization			
β/M_p^4	$<7\times10^{-13}$ for any parametrization			
ϕ_0/M_p	$<1\times10^{-3}$ for any parametrization			
M/M_p	<1 (from prior, Eq. (5.14))			
ε_1	0.04 ± 0.02	0.06	0.00 ± 0.02	0.00
ε_2	0.28 ± 0.13	0.05	0.01 ± 0.08	-0.02
ε_3	-2.3 ± 0.4	-3.1	0.01 ± 0.72	0.87
ε_4	essentially unconstrained			

is the decrease of $dn/d\ln k$ with k. In the $N = 2$ case the value of the running of the spectral index is fairly constant in the region of k accessible to observations. Thus the model (for not too small A, which would lead back to the LOG scenario) approximately resembles the $dn/d\ln k =$ constant standard parametrization. We empirically know from the WMAP analyses [1, 2] (and our own analysis in this paper) that for this standard parametrization the value of n at $k = k_0$ cannot be very far from $n = 1$. This implies from Equations. (4.19), (4.18) and the smallness of q that A cannot be far from $A \sim (2N+3)^{-1/(N+2)}$, which explains the value $A \sim 0.6$. The running $dn/d\ln k$ is then determined by N_e^0 [see equation (4.19)]. Not surprisingly, the preferred value for the running turns out to be consistent with the one from the standard parametrization (compare Tables 1 and 3), which corresponds to the value of N_e^0 quoted above. This is also consistent with our discussion of the (too small) number of e-folds in the standard parametrization. Some of these features are illustrated in Figure 5 (left panel), which shows the interplay of N_e^0 and A and their impact on the spectral index; and Figure 6, which shows the best–fit $n(k)$ (left panel) and the curve corresponding to the posterior mean, alongside with the favoured 95% posterior region of $n(k)$ for $N = 2$. The corresponding $P_s(k)$ is shown in the right panel.

Note that the number of free parameters is essentially the same for both the LOG+NRO case and the constant running parametrization: 4 for the latter (3 if r is set to zero) and 5 for LOG+NRO$\mathcal{F}$ (among which q is almost irrelevant and N has been fixed), and their best–fit log–likelihoods are similar. We comment further on this in Section 7.

Further enforcing a sufficient number of e–folds by imposing a Gaussian prior on N_e^0 (LOG+NRO$\mathcal{G}$ case in Table 3) results in a worsening of the quality of fit (an increase of minus twice the best–fit log–likelihood by 2.1 with respect to the standard power–law case). This is because a larger N_e^0 for a given A implies a spectrum closer to scale–invariance, which is rather strongly disfavoured by data (for example, [14] reports an evidence of 17:1 against a scale invariant spectrum).

As observed in the LOG case, also in the LOG+NRO case the strong degeneracy among the potential parameters makes it impossible to robustly translate the constraints on $\mathbb{P}_{\rm LOG+NRO}$ into prior–independent constraint for the potential parameters, (3.5). As we have done above, we can still define well constrained directions in the subspace spanned by the parameters $\zeta = (\ln\hat{\rho}_0, \ln\hat{q}, \ln\hat{\phi}_0, \ln\hat{M})$ (hats indicate that the variables have been shifted by their posterior mean and normalized to their posterior standard deviation). The eigenvalues of the 3 well–constrained directions are now $\sqrt{\lambda_1} = 0.02$, $\sqrt{\lambda_2} = 0.08$, $\sqrt{\lambda_3} = 0.72$ while $\sqrt{\lambda_4} \gg 1$, and the corresponding rotation matrix is

$$U = \begin{pmatrix} 0.49 & -0.56 & 0.43 & 0.51 \\ -0.84 & -0.05 & 0.23 & 0.53 \\ 0.31 & 0.79 & 0.04 & 0.54 \\ 0.04 & -0.26 & -0.87 & 0.42 \end{pmatrix}. \tag{6.6}$$

Figure 7 shows marginalized 1–dimensional posterior distributions for some of the well constrained parameters in the LOG+NRO ($N = 2$) scenario. Since the value of the tilt, running and running of the running at the pivotal scale are not really representative of the functional form of $n(k)$ in this case, we do not show pdf's for those quantities (even though

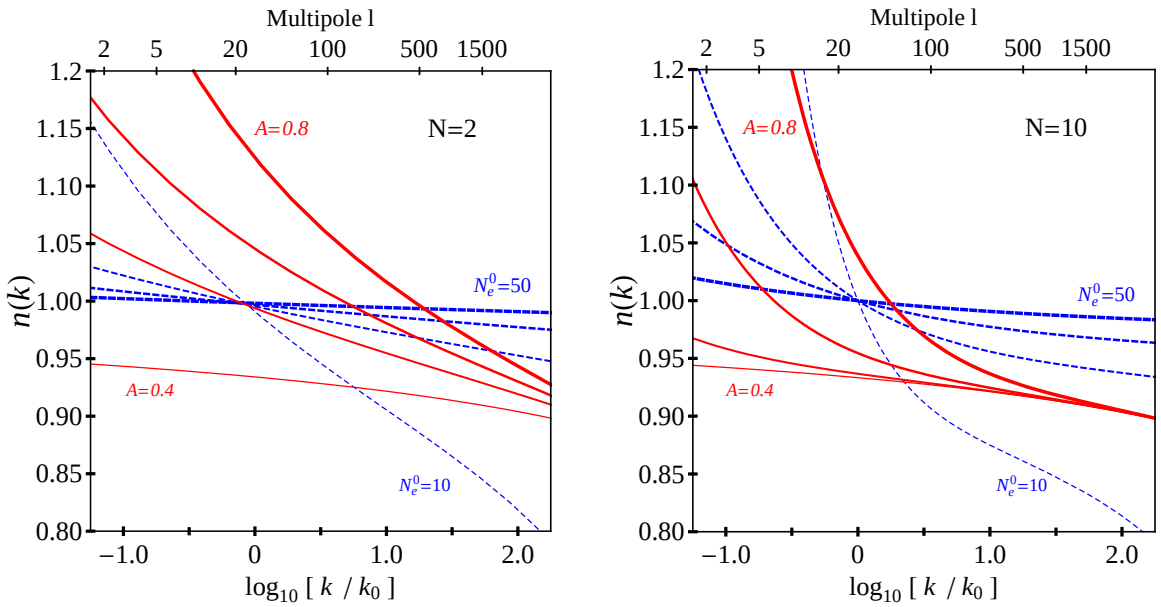

Figure 5: Dependence of $n(k)$ on the parameters N_e^0 (blue, from thin to thick $N_e^0 = 10, 20, 30, 50$, for fixed $A = 0.6$ in the $N = 2$ case, left, and for fixed $A = 0.77$ in the $N = 10$ case, right) and on A (red, from thin to thick $A = 0.2, 0.4, 0.6, 0.8$, for fixed $N_e^0 = 15$ in both panels) in the LOG+NRO scenario with N as indicated.

their constraints are reported for completeness in Table 3). A more faithful representation is actually given in Figure 6.

Let us now turn to the $N = 10$ case. The main difference with the previous $N = 2$ case is that the effect of NRO is much more pronounced on large scales. In particular the running $dn/d\ln k$ can now be quite large at very low k and decrease very quickly, converging to the LOG scenario. Thus, the scenario is qualitatively different from the constant running standard parametrization. As for $N = 2$, the value of q is small and below the theoretically expected bound given by equation (5.23), which translates again into a negligible tensor contribution ($r_0 < 3 \times 10^{-4}$). The preferred value of A is still approximately determined by the empirical condition $n_0 \sim 1$. From Equations. (4.19), (4.18), this translates into $A \sim (2N+3)^{-1/(N+2)} \sim 0.77$. The fact that the model rapidly converges to the LOG scenario allows to increase the number of e-folds to values similar to those of the LOG$\mathcal{F}$ case. More precisely, in the LOG+NRO$\mathcal{F}$ case, the probability distribution for the number of e–folds has a heavier tail for large values of N_e^0, and the 2–tails posterior 68% (95%) region is given by $18.8 < N_e^0 < 37.1$ ($15.8 < N_e^0 < 69.5$), which appears to be solving the horizon problem within 2σ.

Some of these features are illustrated Figure 8. Note in particular that the running of running for the best fit (yellow line in Fig. 8) is positive and sizeable. The quality of the fit is similar to the constant running case for the standard parametrization (though the actual shape of the spectrum is quite different!), although slightly worse. This is not surprising. From subsection 6.1 we know that data prefer a negative second derivative, which cannot be achieved in the LOG+NRO scenario at low k [see discussion after equation (4.19)].

Table 4: As in Table 3 but for $N = 10$ in the LOG+NRO scenario. We did not perform in this case a Principal Component Analysis as for $N = 2$.

Model	LOG+NRO$\mathcal{G}$		LOG+NRO$\mathcal{F}$	
$-2\Delta \ln \mathcal{L}$	2.1		-1.8	
	1D 68%	Best fit	1D 68%	Best fit
Cosmological parameters				
$\Omega_b\, h^2 \times 10^2$	2.31 ± 0.05	2.30	2.23 ± 0.07	2.19
$\Omega_c\, h^2$	0.107 ± 0.004	0.107	0.107 ± 0.004	0.108
Θ_*	$1.044^{+0.003}_{-0.002}$	1.044	1.041 ± 0.003	1.041
τ	0.105 ± 0.026	0.104	$0.089^{+0.014}_{-0.030}$	0.93
H_0 [Km s^{-1}Mpc^{-1}]	74.6 ± 1.6	74.5	73.1 ± 1.8	72.1
Power spectra parameters				
$\ln(P_s^0 \times 10^{10})$	3.14 ± 0.05	3.14	3.15 ± 0.05	3.16
N_e^0	48.2 ± 5.1	48.7	$28.5^{+8.6}_{-9.6}$	17.5
A	$0.52^{+0.19}_{-0.16}$	0.54	$0.57^{+0.17}_{-0.20}$	0.77
q	$< 2 \times 10^{-3}$ for any parametrization			
Derived power spectra parameters				
n_0	$0.982^{+0.002}_{-0.004}$	0.980	0.971 ± 0.016	1.002
$\mathrm{d}n/\mathrm{dln}k\big\vert_{k_0} \times 10^2$	$-0.11^{+0.09}_{-0.06}$	-0.05	$> -3.4\,(95\%)$	-4.17
$\mathrm{d}^2n/\mathrm{dln}^2k\big\vert_{k_0} \times 10^3$	$0.13^{+0.11}_{-0.18}$	-0.03	$< 17.8\,(95\%)$	23.7
r_0	$< 3 \times 10^{-4}$ for any parametrization			
Potential parameters				
ρ/M_p^4	$< 1 \times 10^{-11}$ for any parametrization			
β/M_p^4	$< 1 \times 10^{-14}$ for any parametrization			
ϕ_0/M_p	< 0.2 for any parametrization			
M/M_p	< 1 (from prior, Eq. (5.14))			

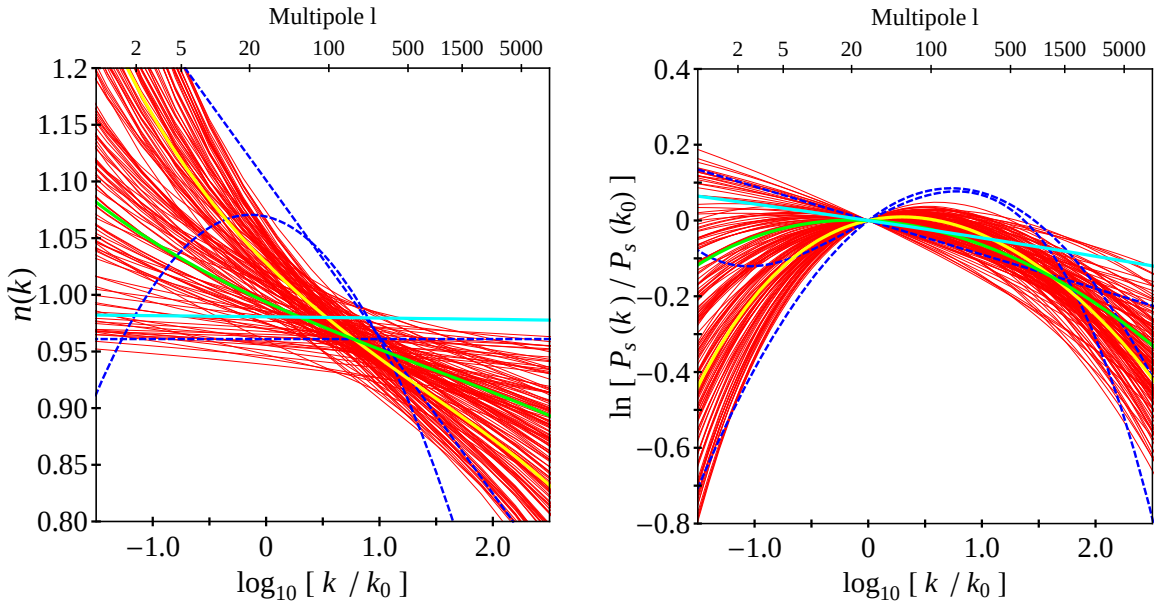

Figure 6: Preferred shape of the spectral index $n(k)$ (left) and the corresponding power spectrum (right) from CMB and LSS data (at 95%, red curves) in the LOG+NRO scenario for $N = 2$. The yellow line shows the best–fit value, the green line the posterior mean while the cyan line is the best–fit further imposing a Gaussian prior on the number of e–folds (LOG+NRO$\mathcal{G}$ scenario). The dotted blue lines represent for reference the best–fit power spectra in the standard parametrization with tilt only, with running and with running of the running (from top to bottom on the right–hand side of the $n(k)$ panel, from top to bottom on the left–hand side of the $P_s(k)$ panel, compare Table 1).

However, as explained there, if the spectral index really runs, a positive second derivative can be much more satisfactory from the physical point of view, in particular to produce a reasonable number of e-folds. This is precisely the case here.

If one enforces a Gaussian prior around $N_e^0 = 50$ (LOG+NRO$\mathcal{G}$ case), then the best–fit spectrum becomes again featureless (light blue, solid line in Figure 8) but with a smaller tilt than the standard parametrization ($n_0 = 0.980$ for the $N = 10$ LOG+NRO$\mathcal{G}$ case), which in turn means that the goodness of fit becomes worse than the standard case (see Table 4). Actually the model becomes in this case quite similar to the simpler LOG$\mathcal{G}$ scenario.

Finally, for values of N between 2 and 10 we have found that the behaviour is intermediate between the cases discussed in the text.

The above discussion shows that there are cases where the standard Taylor expansion of $n(k)$ fails to capture the physics of the models. Generally, the LOG+NRO scenario predicts a running of n which is stronger on large scales. This can only be recovered with several terms in the Taylor expansion, which results in a higher number of free parameters in the fit. On the other hand, the functional form of $n(k)$ in the LOG+NRO scenario implies the positiveness of the second derivative in most of the parameter space, unlike the standard fit. These facts make it impossible to use the results of the standard fits

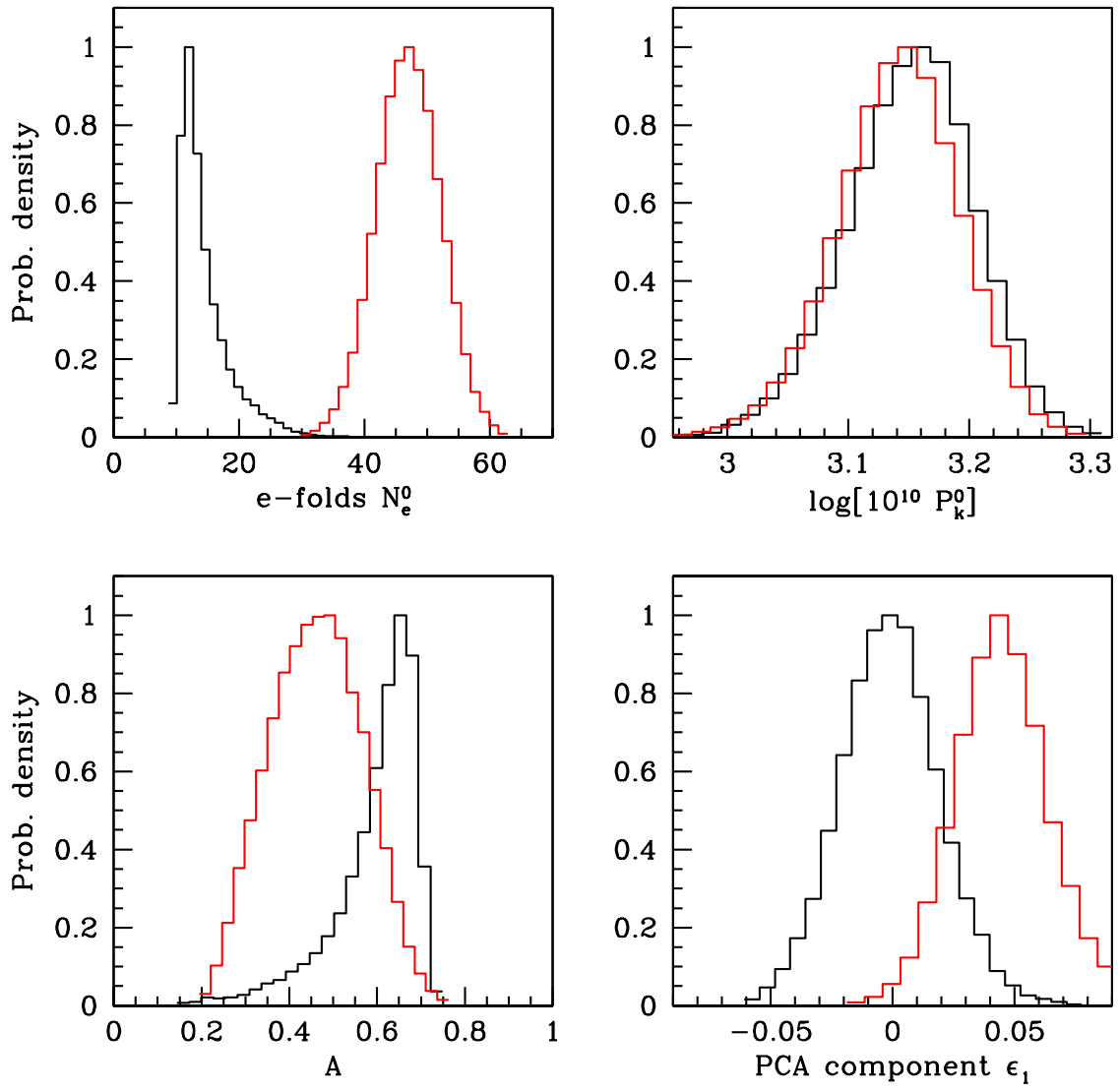

Figure 7: 1D marginalized probability distributions for some well–constrained parameters in the LOG+NRO scenario, for $N = 2$ (compare Table 3). Black curves are for the case with a flat prior on N_e^0, while red is for the case where a Gaussian prior around $N_e^0 = 50$.

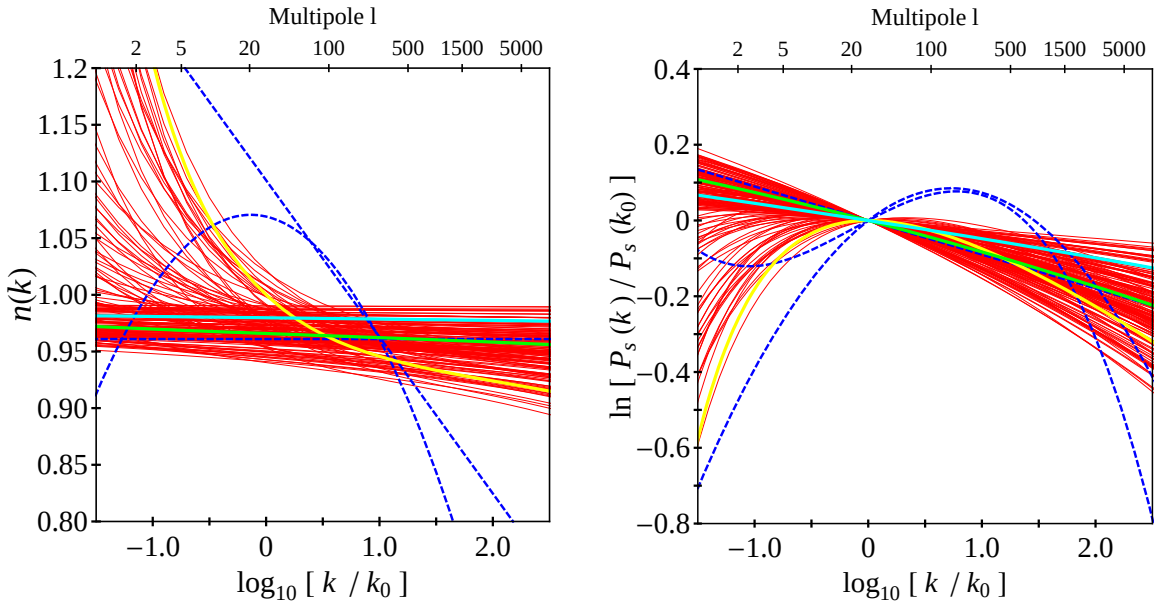

Figure 8: As in Figure 6 but for the LOG+NRO scenario with $N = 10$.

to constrain the LOG+NRO scenario: a direct comparison of the model with the data becomes necessary (as we have done here). This situation could easily apply to other theoretical models, as well, and therefore great caution is necessary when interpreting generic constraints on the coefficient of the standard Taylor expansion in terms of specific physical models.

7 Model comparison

In the previous section we have presented parameter constraints for each class of model, namely the phenomenological model in the standard parametrization and the more physically motivated LOG and LOG+NRO scenarios. Assessing the relative performance of the three models is a model comparison question, to which we now turn our attention.

In the traditional frequentist approach to statistics, model comparison is tackled in terms of hypothesis testing: for example, we might ask whether the improvement in the best–fit likelihood in terms of the effective $\Delta\chi^2 = -2\Delta \ln \mathcal{L}$ when adding a running to the tilt is "significant" enough to warrant the inclusion of a non–zero running. There are however several reasons why answering this question is far from trivial. A technical reason is that the usual rule of thumb of "$\Delta\chi^2$ per extra degree of freedom" can only be applied if certain regularity conditions are met, and in particular only if the extra parameter for nested model does not lie on the boundary of the parameter space (see [35] for an astrophysical example and references therein). So for example, the $\Delta\chi^2$ criterion could not be applied to compare the quality of fit of the LOG model with that of LOG+NRO, since the former is obtained from the latter by setting $A = 0$, and $A < 0$ is not allowed.

Another, more fundamental aspect has to do with the meaning and interpretation of

frequentist hypothesis testing. As discussed in detail in [13], frequentist likelihood ratio tests *assume* the hypothesis $\mathcal{H}$ is true and give the probability of observing data d as extreme or more extreme than what has actually been measured. This is a statement on the probability of the data assuming a hypothesis $\mathcal{H}$ to be true (which in Bayesian terms amounts to the choice of a model, $\mathcal{M}$), i.e. frequentist hypothesis testing gives $P(d|\mathcal{H})$. But this is not the quantity one is usually interested in, which is actually $P(\mathcal{M}|d)$, the probability of the model $\mathcal{M}$ given the observations, which can only be obtained by using Bayes theorem to invert the order of conditioning. For this reason, model selection is an inherently Bayesian question [14].

Bayesian model selection is based on the computation of the model likelihood $P(d|\mathcal{M}) \equiv \mathcal{E}(\mathcal{M})$ (also called "evidence"), which is the normalization constant in the denominator of Bayes theorem (see [14, 36] for details) obtained by averaging the likelihood $P(d|\theta, \mathcal{M})$ over the prior $P(\theta|\mathcal{M})$ in the parameter space θ of the model

$$\mathcal{E}(\mathcal{M}) = \int P(d|\theta, \mathcal{M}) P(\theta|\mathcal{M}) d\theta. \tag{7.1}$$

From the model likelihood one obtains the model probability given the data by using once more Bayes theorem, $P(\mathcal{M}|d) \propto P(\mathcal{M})\mathcal{E}(\mathcal{M})$, where $P(\mathcal{M})$ is the prior probability assigned to the model (usually taken to be noncommittal and equal to $1/N_m$ if one considers N_m different models). When comparing two models one usually computes the Bayes factor B_{12}, given by the ratio of the evidences between the two models:

$$\ln B_{12} = \ln \mathcal{E}(\mathcal{M}_1) - \ln \mathcal{E}(\mathcal{M}_2). \tag{7.2}$$

The Bayes factor thus gives the factor by which the relative odds among two models have changed after the arrival of the data. As a simple calculation shows for the case of Gaussian likelihood and prior, equation (7.1) contains both a likelihood ratio term which rewards better fitting, and an "Occam's razor" term that disfavours unnecessary model complexity, defined in terms of useless parameters (see [37] for a discussion of model complexity). The "best" model is one that combines good fitting with model predictivity. Bayes factors are usually interpreted against the Jeffreys' scale for the strength of evidence, which we qualify as follows: "weak evidence" for $|\ln B| < 2.5$, "moderate evidence" for $2.5 < |\ln B| < 5.0$ and "strong evidence" for $|\ln B| > 5.0$. The computation of the model likelihood is in general a numerically difficult task, as it involves a multi–dimensional integration over the whole of parameter space. Furthermore, a prior dependence is (correctly) built into the method, as the Occam's razor term depends on the ratio of the prior to posterior volume, which gives the amount of "wasted" parameter space of the model. Therefore it is problematic to evaluate the Bayes factor unless one has a physically motivated way of setting the prior volume.

The difficulty of using a fully Bayesian approach to the comparison of the standard Taylor series parametrization with either the LOG or the LOG+NRO scenario is that the former represents a purely phenomenological fit to the data, while the LOG and LOG+NRO models are physically motivated. In particular, setting a prior on the potential parameters of the LOG and LOG+NRO models is not comparable to setting a strictly phenomenological prior on the quantities of direct relevance for the fit, i.e. the spectral

tilt, the running, etc., in the standard parametrization. The Occam's razor effect which rewards highly predictive models does not work properly if we do not compare like with like, i.e. if we are unable to set priors on the parameter space of the phenomenological parametrizations used for the fit. Since the standard parametrization is by construction phenomenological, it cannot be directly compared using the Bayesian evidence to the LOG and LOG+NRO scenarios.

However, we can still draw some interesting, partial conclusion from a Bayesian approach. In ref. [13], a method was presented to derive upper bounds on the Bayesian evidence for nested models, called "Bayesian calibrated p–values", that is useful in cases such as this where there is only a very loose physical basis to assign priors to phenomenological quantities in the fit (here, the various terms in the expansion of the potential). This allows to assess whether extra parameters are unnecessary within the framework of nested models, as it gives the Bayes factor which (under mild assumptions) *maximizes* the evidence in favour of the more complex model (i.e., with more terms in the Taylor expansion). If this turns out to be not very strong, then one can confidently conclude that the extra parameters are not needed.

Table 5: Summary of model comparison statistics. Wherever the Bayes factor is given, the notation $\ln B_{ij}$ indicated the Bayes factor between model i and model j (with $\ln B_{ij} > 0$ favouring model i). An overbar indicates a prior–independent upper limit obtained using the Bayesian calibrated p–values method. The quantity n gives the number of effective parameters in the model.

Model	$\Delta\chi^2$	n	> 50 e–folds?	Bayes factor	Notes
Standard parametrization					
no running	0.0	3(+1)	ad hoc	—	
with running	-3.4	4(+1)	ad hoc	$\ln \bar{B}_{21} = 0.7$	No evidence
running of running	-4.4	5(+1)	ad hoc	$\ln \bar{B}_{32} = 0.0$	No evidence
				$\ln \bar{B}_{31} = 0.4$	No evidence
LOG models					
LOG$\mathcal{F}$	-0.4	~ 2	yes (at 2σ)	—	
LOG$\mathcal{G}$	$+2.1$	~ 1	yes	$\ln \bar{B}_{45} = 0.4$	
LOG+NRO models					
LOG+NRO$\mathcal{F}$, $N = 2$	-2.7	~ 3	no	—	Excluded
LOG+NRO$\mathcal{G}$, $N = 2$	$+2.4$	~ 2	yes	—	Disfavoured
LOG+NRO$\mathcal{F}$, $N = 10$	-1.8	~ 3	yes (at 2σ)	$\ln B_{84} \sim 0.0$	Au par LOG$\mathcal{F}$
LOG+NRO$\mathcal{G}$, $N = 10$	$+2.1$	~ 2	yes	$\ln B_{95} < -2.3$	Disfavoured

Table 5 summarizes some relevant model comparison statistics. Focusing first on the "standard parametrization" section, we have employed the method of ref. [13] to derive a prior–independent upper bound on the Bayesian evidence in favour of extra terms in the Taylor expansion. The maximum Bayesian evidence in favour of a running is only $\ln \bar{B}_{21} = 0.7$ (compared to a model with just a spectral tilt), which falls short of even the "weak evidence" threshold. The maximum evidence in favour of a third term in the Taylor expansion is even weaker. We can therefore conclude that, for the standard parametrization, present data do not require any higher order terms than a spectral tilt (for which ref. [13] found a maximum evidence of $\ln \bar{B} = 2.9$ compared to a scale–invariant spectrum). Notice that in this phenomenological approach the number of e–folds has to be added in by hand as an extra parameter of the model (although it would be derivable given a specific enough model for the inflaton potential), indicated as (+1) in the column giving an approximate value of the effective number of parameters in the model.

Regarding the LOG class of models, the goodness of fit of the LOG$\mathcal{F}$ case is similar to the one of the simple tilt model. Although the number of free parameters of the LOG scenario is 3, the parameter q is irrelevant to the fit and therefore the effective number of parameters is closer to 2. A more precise counting of the effective parameters could be achieved using the notion of Bayesian complexity [37], but this is not required in the context of the present discussion. It is interesting to notice that the LOG scenario also solves the horizon problem (within 2σ of the posterior mean) with an extreme economy of free parameters. The LOG$\mathcal{G}$ case dispenses with one further parameter (as N_e^0 becomes almost fixed to $N_e^0 \sim 50$) and the upper bound on the Bayesian evidence in favour of LOG$\mathcal{F}$ indicates that the difference of $\Delta\chi^2 = 2.5$ between the flat and Gaussian prior on N_e^0 is not strongly significant.

The LOG model can be considered nested within the LOG+NRO class of models, with the former formally obtained from the latter by setting $A = 0$. For $N = 2$, the LOG+NRO$\mathcal{F}$ model falls short of achieving the necessary number of e–folds, and for this reason it must be excluded, even though its quality of fit is comparable to the standard case with constant running. The LOG+NRO$\mathcal{G}$ case has one extra parameter (for fixed N) than LOG$\mathcal{G}$, and a best–fit value which is actually slightly worse, a consequence of the Gaussian prior forcing the posterior distribution around a value of N_e^0 which is not strongly favoured by the data. Hence we can conclude that LOG+NRO$\mathcal{G}$ ($N = 2$) is disfavoured with respect to LOG$\mathcal{G}$ and LOG$\mathcal{F}$ since it is unable to achieve a better fit even with one extra parameter.

The LOG+NRO$\mathcal{F}$ with $N = 10$ has a better fit than the LOG scenario and it achieves a sufficient number of e–folds within 2σ. The method of Bayesian calibrated p–values cannot be used to compare the two models because the LOG model (obtained by setting $A = 0$ in the LOG+NRO model) lies at the boundary of parameter space. However, we can still roughly estimate the Bayes factor between LOG$\mathcal{F}$ and LOG+NRO$\mathcal{F}$ by taking a prior width on the extra parameter A of order unity (as motivated by the theoretical expectations presented in Section 5.2) and using that, for nested models, the Bayes factor in favour of the simpler model is approximately (see equation (9) in [14])

$$\ln B \sim I - \lambda^2/2, \tag{7.3}$$

where I is the logarithm of the ratio of the prior to posterior volume (the information gain) for the extra parameter and λ is the number of sigmas discrepancy between the likelihood peak and the value of the extra parameter under the nested model (here, $A = 0$). Using the values in Table 4 one obtains $\lambda \sim 2.8$ and $I \sim 1.6$ and thus $\ln B \sim -2.3$, which would weakly favour the LOG+NRO$\mathcal{F}$ model. However, one has to bear in mind that the parameter N has been fixed to a value picked among a range of order 10 possible values — hence one has to factor in an extra Occam's razor effect coming from the fact that $N = 10$ is one of about 10 possible choices for N. Hence $\ln B$ has to be increased by about a factor $\ln 10 = 2.3$, which brings the final odds between LOG+NRO$\mathcal{F}$ and LOG$\mathcal{F}$ to unity (i.e., $\ln B \sim 0$). Finally, the LOG+NRO$\mathcal{G}$ case has the same quality of fit of the LOG$\mathcal{G}$ case and one extra parameter. The Occam's razor term from the choice of N alone would disfavour LOG+NRO$\mathcal{G}$ by a factor $\ln B = 2.3$ with respect to LOG$\mathcal{G}$, so even without computing the precise Bayes factor we can conclude that this scenario is disfavoured.

In conclusion, a model comparison approach singles out the LOG scenario and the LOG+NRO$\mathcal{F}$ ($N = 10$) model as the most viable cases in light of the present data. This kind of considerations could be extended to compare this class of models with other inflationary scenarios, once they have been suitably parametrized in terms of fundamental variables. However, a direct comparison with a phenomenological approach such as the standard Taylor expansion of the spectrum is not feasible due to the lack of predictivity of the latter. The Bayesian evidence still concludes that no higher–order term than the tilt is presently required in the series.

Finally, we emphasize that the LOG and LOG+NRO models predict tensor contributions that are generally very small and will be largely undetectable. The most optimistic case is the LOG, where the upper bound is of order $r_0 \sim 10^{-3}$, which might be just within reach of future B–modes observations. Conversely, a detection of tensor modes above $\sim 10^{-3}$ would disprove the scenario of flat tree–level inflationary potentials.

8 Conclusions

In this paper we have compared a broad and physically well-motivated class of inflationary models with CMB and LSS observational data. Namely, we have considered models with flat tree-level potentials, which typically appear in supersymmetric theories, where $V_{\rm tree}^{\rm SUSY}$ ordinarily has plenty of accidental flat directions. These models, beside being very well motivated from the physical point of view (on a similar footing to monomial potentials), lead to very model-independent cosmological predictions. The reason is that the potential derivatives V', V'',... arise from the radiative corrections to V, which has a characteristic logarithmic dependence on the inflaton field. This scenario has been labelled "LOG" throughout the paper. In addition, we have considered the possible presence of new physics beyond a certain high-energy cut-off. This physics does not need to respect the flat directions of the "low-energy" theory, and thus it will show up as non-renormalizable operators (NRO) in the inflaton field, which will be dominated by the lowest–order one. This modified scenario (labelled "LOG+NRO") is also very well motivated and still quite

model-independent.

We have studied the performance of these scenarios when compared with CMB and LSS. We have made first a detailed study of the features of these models, working out both numerically accurate results and approximate analytical expressions for $P_s(k)$, $P_t(k)$ and other relevant quantities, such as the spectral index, $n(k)$, as a function of suitably defined model parameters. We also discussed the number of independent parameters and the theoretical and phenomenological constraints on them (to be imposed a priori). As a matter of fact, one (combination) of the parameters is almost irrelevant, which makes these models even more predictive. Another parameter is essentially the number of e-folds, N_e^0, since the time when the largest observable scales crossed out the horizon until the end of inflation. This allows to perform the fits in a twofold way: either leaving N_e^0 free, and let the data determine its value, or imposing a prior on its value according to the usual theoretical prejudice ($N_e^0 = 50 - 60$). Both approaches (labelled $\mathcal{F}$ and $\mathcal{G}$ respectively) are interesting and complementary.

In the analysis we also study the performance of standard parametrizations of the power spectrum, based on a Taylor expansion of $\ln P_s(k)$ and $\ln P_t(k)$ around an (arbitrary) pivotal scale, $\ln k_0$. At first (second) order these parametrizations correspond to a constant (constantly running) spectral index, $n(k) =$ constant ($dn/d\ln k =$ constant). They have been used in reference analyses, in particular by the WMAP collaboration. It is important to keep in mind that, although useful, the standard parametrizations are not inspired by any particularly well-motivated inflationary physics. E.g. the results of the fit with the $dn/d\ln k =$ constant assumption are not consistent with a number of e-folds in the required range. Still we have also studied them (going one order beyond the WMAP analysis) to facilitate the discussion of the performance of the LOG and LOG+NRO scenarios. As a general comment, care must be taken to test inflationary models which predict a non-negligible scale dependence. In many cases the standard Taylor series parametrization of equations (2.9) and (2.10) cannot be accurately used in such a situation unless a high number of terms is taken in the expansion.

Our main results are the following:

- Both the LOG and LOG+NRO scenarios predict small tensor perturbations: $r_0 \leq \mathcal{O}(10^{-3})$.
- The LOG scenario has essentially two parameters, $P_s(k_0)$ and N_e^0, and implies a nearly constant $n(k)$.
- Leaving N_e as a free parameter (LOG$\mathcal{F}$ fit), one gets $24 < N_e^0 < 49$ ($16 < N_e^0 < 84$) at 68% (95%) c.l. while the corresponding spectral index is close to $n_0 = 0.96$. This result is consistent with the theoretical prejudice $N_e^0 \sim 50-60$, required to solve the horizon problem, which is remarkable. In the LOG$\mathcal{G}$ fit (i.e. imposing $N_e^0 = 50-60$) one gets $n_0 \simeq 0.98$. Note that this fit has only one parameter and still works very well.
- The LOG+NRO scenario has two more parameters, which arise from the order and the suppression scale of the NRO. We have fixed the order of the NRO (denoted 4+

$2N$ throughout the paper) to two representative values ($N = 2, 10$) that reasonably encompass the sensible physical range. Thus in practice we are playing with just one additional parameter. This scenario can produce a sizeable running of the spectral index, and still be consistent with the data and a reasonable number of e-folds, especially if N is not very small. The impact of the NRO (driving a running of the spectral index) is relevant at small k, corresponding to the first stages of the inflationary period, and then it quickly converges (especially for not too small N) to the LOG scenario.

- The model comparison is delicate for several technical and fundamental reasons. In the paper we give a fully Bayesian discussion of the relative quality of the various scenarios considered. Qualitatively, it can be said that the goodness of the LOG (NRO+LOG$\mathcal{F}$) fits is similar to the standard $n =$ constant ($dn/d\ln k =$ constant) parametrization. The improvement in the goodness of the fit obtained by the inclusion of an extra parameter (as the LOG+NRO scenario implies) is not enough (with the present data) to justify such modification, but still it remains an interesting theoretical possibility. On the other hand, a rigorous comparison between the evidences for LOG, LOG+NRO scenarios and for the standard parametrizations (which are phenomenological by construction) is not feasible. However, the prior–independent method of the Bayesian calibrated p–values still indicates that no higher order term than a tilt is required in the standard Taylor expansion.

As a final conclusion, the LOG and LOG+NRO scenarios analyzed in this paper (based on flat tree-level potentials without or with the presence of extra physics) are not only very well motivated from the physical point of view, but they also fit remarkably well the CMB and LSS data, with very few parameters (the predictions are quite model independent). In addition they are naturally consistent with a reasonable number of e-folds. Therefore, they can be considered as a standard physical class of inflationary models, on a similar footing as monomial potentials.

A Some complementary formulas

In this appendix we provide some important expressions for the case of the potential with NRO. Applying the following two identities of hypergeometric functions:

$$\begin{aligned} {}_2F_1(a,b;c;z) &= {}_2F_1(b,a;c;z) \\ {}_3F_2(a,b,c;a+1,b+1;z) &= \frac{1}{b-a}\left[b\,{}_2F_1(a,c;a+1;z) - a\,{}_2F_1(b,c;b+1;z)\right] \end{aligned}$$

one can see, integrating equation (2.5), that

$$\begin{aligned} \ln\frac{k}{k_0} &\simeq -\frac{q}{2}N_e^0\varphi\left\{\frac{1}{N+2}+\left(\frac{2}{q}-\frac{1}{N+2}+\ln\varphi\right){}_2F_1\left(\frac{1}{N+2},1;\frac{N+3}{N+2};-(A\varphi)^{N+2}\right)\right. \\ &+ \frac{N+2}{(N+1)^2}\left[(A\varphi)^{-N-2}\left(1-(A\varphi)^{N+2}\right)^{-\frac{1}{N+2}}+\left(1-(A\varphi)^{N+2}\right)^{-\frac{1}{N+2}}\right. \\ &- \left.\left.(A\varphi)^{-N-2}-(N+1){}_2F_1\left(\frac{1}{N+2},\frac{1}{N+2};\frac{N+3}{N+2};-(A\varphi)^{N+2}\right)\right]\right\}\Bigg|_{\varphi=1}^{\phi^2/\phi_0^2} \end{aligned} \tag{A.1}$$

being the slow-roll approximation the only reason for the symbol of approximate equality. The expression (4.15) that we use in the fits is directly obtained from (A.1) neglecting the irrelevant addends, i.e. all but the one that is not proportional to the small parameter q.

The first order slow-roll parameters in this scenario are:

$$\epsilon = \frac{1}{4qN_e^0\,\Phi}\left[\frac{1+(A\,\Phi)^M}{\frac{1}{q}+\frac{1}{2M}(A\,\Phi)^M+\frac{1}{2}\ln\Phi}\right]^2 , \tag{A.2}$$

$$\eta = \frac{1}{2qN_e^0\,\Phi}\left[\frac{(2M-1)(A\,\Phi)^M-1}{\frac{1}{q}+\frac{1}{2M}(A\,\Phi)^M+\frac{1}{2}\ln\Phi}\right] , \tag{A.3}$$

where we have defined

$$\Phi \equiv \left(\frac{\phi}{\phi_0}\right)^2 , \tag{A.4}$$

to simplify the notation. Notice that in the limit of the NRO going to zero we recover the formulas (4.1).

The relation between $\mathbb{P}_{\rm LOG+NRO}$ and the physical parameters of the potential are given by:

$$\phi_0/M_p = \sqrt{2qN_e^0}\,, \tag{A.5}$$

$$\rho/M_p^4 = 48\pi^2 q(N+2)^3\frac{P_s^0}{N_e^0}\frac{\left(1+A^{N+2}\right)^2}{\left[2(N+2)+qA^{N+2}\right]^3}\,, \tag{A.6}$$

$$\beta/M_p^4 = 48\pi^2 q^2(N+2)^3\frac{P_s^0}{N_e^0}\frac{\left(1+A^{N+2}\right)^2}{\left[2(N+2)+qA^{N+2}\right]^3}\,, \tag{A.7}$$

$$M/M_p = \sqrt{2qN_e^0}\left\{6\pi^2(N+2)^2\frac{P_s^0}{N_e^{0\,3}}\frac{A^{N+2}\left(1+A^{N+2}\right)^2}{\left[2(N+2)+qA^{N+2}\right]^3}\right\}^{-\frac{1}{2N}} . \tag{A.8}$$

Acknowledgments

We thank Cédric Delaunay, Massimiliano Lattanzi, Mischa Salle and Licia Verde for interesting discussions. This work is supported by the Spanish Ministry of Education and Science through the research project FPA2004-02015; by a Comunidad de Madrid project (P-ESP-00346); by a Marie Curie Fellowship of the European Community under contract MEST-CT-2005-020238-EUROTHEPY; and by the European Commission under contracts MRTN-CT-2004-503369 and MRTN-CT-2006-035863 (Marie Curie Research and Training Network "UniverseNet"). We also acknowledge the use of the IFT Beowulf cluster funded by the CM project above. G.B. would like to thank the hospitality of Oxford Astrophysics and Theoretical Physics for a research stay during which this work was partly conducted. He also acknowledges financial support from the Comunidad de Madrid and the European Social Fund through a FPI contract. R. RdA is supported by the program "Juan de la Cierva" of the Ministerio de Educación y Ciencia of Spain. R.T. is supported by the Royal Astronomical Society through the Sir Norman Lockyer Fellowship and by St Anne's College, Oxford.

References

[1] H. V. Peiris *et al.* [WMAP Collaboration], "First year Wilkinson Microwave Anisotropy Probe (WMAP) observations: Implications for inflation," Astrophys. J. Suppl. **148** (2003) 213 [astro-ph/0302225].

[2] D. N. Spergel *et al.* [WMAP Collaboration], "Wilkinson Microwave Anisotropy Probe (WMAP) three year results: Implications for cosmology," Astrophys. J. Suppl. **170** (2007) 377 [astro-ph/0603449].

[3] A. H. Guth, "The Inflationary Universe: A Possible Solution To The Horizon And Flatness Problems," Phys. Rev. D **23** (1981) 347.

[4] V. F. Mukhanov and G. V. Chibisov, "Quantum Fluctuation And Nonsingular Universe. (In Russian)," JETP Lett. **33** (1981) 532 [Pisma Zh. Eksp. Teor. Fiz. **33** (1981) 549].

[5] A. A. Starobinsky, "Dynamics Of Phase Transition In The New Inflationary Universe Scenario And Generation Of Perturbations," Phys. Lett. B **117** (1982) 175.

[6] S. W. Hawking, "The Development Of Irregularities In A Single Bubble Inflationary Universe," Phys. Lett. B **115** (1982) 295.

[7] A. H. Guth and S. Y. Pi, "Fluctuations In The New Inflationary Universe," Phys. Rev. Lett. **49** (1982) 1110.

[8] J. M. Bardeen, P. J. Steinhardt and M. S. Turner, "Spontaneous Creation Of Almost Scale - Free Density Perturbations In An Inflationary Universe," Phys. Rev. D **28** (1983) 679.

[9] J. E. Lidsey, A. R. Liddle, E. W. Kolb, E. J. Copeland, T. Barreiro and M. Abney, "Reconstructing the inflaton potential: An overview," Rev. Mod. Phys. **69** (1997) 373 [astro-ph/9508078].

[10] A. R. Liddle, P. Parsons and J. D. Barrow, "Formalizing the slow roll approximation in inflation," Phys. Rev. D **50** (1994) 7222 [astro-ph/9408015].

[11] D. H. Lyth and A. Riotto, "Particle physics models of inflation and the cosmological density perturbation," Phys. Rept. **314** (1999) 1 [hep-ph/9807278].

[12] E. J. Copeland, E. W. Kolb, A. R. Liddle and J. E. Lidsey, "Reconstructing the inflation potential, in principle and in practice," Phys. Rev. D **48** (1993) 2529 [hep-ph/9303288].

[13] C. Gordon and R. Trotta, "Bayesian Calibrated Significance Levels Applied to the Spectral Tilt and Hemispherical Asymmetry," arXiv:0706.3014 [astro-ph].

[14] R. Trotta, "Applications of Bayesian model selection to cosmological parameters," Mon. Not. Roy. Astron. Soc. **378** (2007) 72 [astro-ph/0504022].

[15] Nasa's Legacy Archive for Microwave Background Data Analysis (LAMBDA), http://lambda.gsfc.nasa.gov/

[16] See however J. Hamann, S. Hannestad, M. S. Sloth and Y. Y. Y. Wong, "How robust are inflation model and dark matter constraints from cosmological data?," Phys. Rev. D **75** (2007) 023522 [astro-ph/0611582].

[17] G. Ballesteros, J. A. Casas and J. R. Espinosa, "Running spectral index as a probe of physics at high scales," JCAP **0603** (2006) 001 [hep-ph/0601134].

[18] P. Binetruy and G. R. Dvali, "D-term inflation," Phys. Lett. B **388** (1996) 241 [hep-ph/9606342].

[19] M. Abramowitz and I.A. Stegun, "Handbook of mathematical functions with formulas, graphs, and mathematical tables," Dover Publications, 1968.

[20] A. Lewis and S. Bridle, "Cosmological parameters from CMB and other data: a Monte-Carlo approach," Phys. Rev. D **66** (2002) 103511 [astro-ph/0205436].

[21] A.E. Raftery and S.M. Lewis, "The number of iterations, convergence diagnostics and generic Metropolis algorithms." In *Practical Markov Chain Monte Carlo*, (W.R. Gilks, D.J. Spiegelhalter and S. Richardson, eds.), London, Chapman and Hall.

[22] W. H. Kinney, "How to fool cosmic microwave background parameter estimation," Phys. Rev. D **63**, 043001 (2001) [astro-ph/0005410].

[23] G. Hinshaw *et al.* [WMAP Collaboration], "Three-year Wilkinson Microwave Anisotropy Probe (WMAP) observations: Temperature analysis," Astrophys. J. Suppl. **170**, 288 (2007) [astro-ph/0603451].

[24] C. L. Kuo *et al.*, "Improved Measurements of the CMB Power Spectrum with ACBAR," [astro-ph/0611198].

[25] A. C. S. Readhead *et al.*, "Extended Mosaic Observations with the Cosmic Background Imager," Astrophys. J. **609**, 498 (2004) [astro-ph/0402359].

[26] T. E. Montroy *et al.*, "A Measurement of the CMB Spectrum from the 2003 Flight of BOOMERANG," Astrophys. J. **647**, 813 (2006) [astro-ph/0507514].

[27] M. Tegmark *et al.*, "Cosmological Constraints from the SDSS Luminous Red Galaxies," Phys. Rev. D **74**, 123507 (2006) [astro-ph/0608632].

[28] W. L. Freedman *et al.*, "Final Results from the Hubble Space Telescope Key Project to Measure the Hubble Constant," Astrophys. J. **553**, 47 (2001) [astro-ph/0012376].

[29] S. M. Leach, A. R. Liddle, J. Martin and D. J. Schwarz, "Cosmological parameter estimation and the inflationary cosmology," Phys. Rev. D **66**, 023515 (2002) [astro-ph/0202094].

[30] T. Gherghetta, C. F. Kolda and S. P. Martin, "Flat directions in the scalar potential of the supersymmetric standard model," Nucl. Phys. B **468**, 37 (1996) [hep-ph/9510370].

[31] M. Dine, L. Randall and S. D. Thomas, "Baryogenesis From Flat Directions Of The Supersymmetric Standard Model," Nucl. Phys. B **458**, 291 (1996) [hep-ph/9507453].

[32] M. Cvetic, "Nonrenormalizable Sector of the Effective Lagrangian from Superstring Theories," Presented at Strings '88 Workshop, College Park, Md., Mar 24-28, 1988.

[33] A. Font, L. E. Ibanez, H. P. Nilles and F. Quevedo, "Degenerate Orbifolds," Nucl. Phys. B **307** (1988) 109 [Erratum-ibid. B **310** (1988) 764].

[34] This has also been noted by J. Lesgourgues and W. Valkenburg, "New constraints on the observable inflaton potential from WMAP and SDSS," Phys. Rev. D **75**, 123519 (2007) [astro-ph/0703625].

[35] R. Protassov, D. A. van Dyk, A. Connors, V. L. Kashyap and A. Siemiginowska, "Statistics: Handle with Care, Detecting Multiple Model Components with the Likelihood Ratio Test," [astro-ph/0201547].

[36] R. Trotta, "Forecasting the Bayes factor of a future observation," Mon. Not. Roy. Astron. Soc. **378**, 819 (2007) [astro-ph/0703063].

[37] M. Kunz, R. Trotta and D. Parkinson, "Measuring the effective complexity of cosmological models," Phys. Rev. D **74**, 023503 (2006) [astro-ph/0602378].